Title
Wind, Thermal, and Earthquake Monitoring of the Watts Towers

Author
English, Jackson

Publication Date
2013

Peer reviewed|Thesis/dissertation

UNIVERSITY OF CALIFORNIA

Los Angeles

Wind, Thermal, and Earthquake Monitoring of the Watts Towers

A thesis submitted in partial satisfaction

of the requirements for the degree Master of Science

in Civil Engineering

by

Jackson English

2013

ABSTRACT OF THE THESIS

Wind, Thermal, and Earthquake Monitoring of the Watts Towers

by

Jackson English

Master of Science in Civil Engineering

University of California, Los Angeles, 2013

Professor Ertugrul Taciroglu, Chair

Robert L. Nigbor, Co-chair

The Watts Towers are a National Historic Landmark consisting of 17 interconnected structures built by one artist, Simon Rodia, between 1921 and 1955. As part of an ongoing effort led by the Los Angeles County Museum of Art to preserve the Towers, UCLA engineers have been experimentally and analytically studying how environmental factors affect the structural behavior and crack movements. Measured thermal effects on the tower include shifts in the structure's fundamental frequencies, daily tilting patterns, and daily crack movement. A finite element model was created in order to further study the observed thermal effects. Modeled thermal tilt behavior was consistent with measured results, but the magnitude of tilt was 80-90% lower than measured. Earthquakes and windstorms have previously caused damage to the Towers. The current data set shows that both small earthquakes and moderate winds produce motions exceeding thermal levels. Monitoring will continue to capture larger earthquakes and windstorms.

The thesis of Jackson English is approved.

Jonathan Paul Stewart

John Wright Wallace

Robert L. Nigbor, Committee Co-chair

Ertugrul Taciroglu, Committee Chair

University of California, Los Angeles

2013

Table of Contents

List of Figures

List of Tables

Acknowledgments

Funding for this work was provided by the National Science Foundation through Award CMMI-1331299 with collaboration by the George E. Brown Network for Earthquake Engineering Simulation under Award CMMI-0927178. Any opinions, findings, and conclusions or recommendations expressed in this material are those of the author and do not necessarily reflect the views of the National Science Foundation.

First and foremost, I would like to personally thank all of my friends and family who have supported me through both my undergraduate and graduate time at UCLA. I could not have done it without them. I would like to thank all of the NEES interns and UCLA students who have helped with this project. Specifically, I would like to thank Winston Boyce and Shushoma Sravostee for their help during the summer in the field and in the office. The computer model couldn't have been developed had it not been for the help of Armen Azizian, Evelyn Barkhordarian, and Homa Shahpasandzadeh in processing the laser scan. Murat Uzun's help is also greatly appreciated. Without the tireless work of the nees@UCLA staff including Erica Eskes, Andrey Kozhukhovskiy, Alberto Salamanca, Steve Keowen, and Sophia Poulos, projects such as this one could never happen. My great appreciation is extended to the Los Angeles County Museum of Art, Dr. Frank Preusser, and the rest of his team for allowing the nees@UCLA team to be part of a project with such great historical, cultural, and artistic significance.

I must also extend my gratitude to my thesis committee members Professor John Wallace and Professor Jonathan Stewart. Lastly, I would like to thank Professor Ertugrul Taciroglu (Et), and Professor Robert Nigbor (Bob). I was lucky enough to work with both of them as an undergrad and even luckier that they selected me to work on this Watts Towers project for my master's thesis. Throughout it all, I have learned a lot, but more importantly, I have had a lot of fun.

1 Introduction and Organization

The Watts Towers are a National Historic Landmark and an internationally acclaimed work of art. Located in Los Angeles, California, the Watts Towers stand high above the surrounding landscape, with the tallest structure reaching a height of nearly 100 feet. Throughout this thesis, the three main towers, which can be clearly seen in the far left photograph in Figure 1.1, will be referred to as the East Tower, Center (or Central) Tower, and the West Tower. The Towers were constructed by one person, Simon Rodia, using a wide variety of materials, but maintaining the general design of covering a piece of structural steel with a wire mesh and then covering the mesh with a cement mortar. Preservation efforts on the Towers date back to shortly after Rodia finished his work in 1955 (Goldstone, 1997).

Figure 1.1: Photographs of the Watts Towers: A) view looking south, showing the three towers B) view looking east along the south wall C) view from inside the site, showing parts of the other structures and the overhead arches connecting all around the site

Recently, the Los Angeles County Museum of Art (LACMA) partnered with the City of Los Angeles Department of Cultural Affairs with the goal of developing an updated and comprehensive long-term preservation plan for the Watts Towers. One pressing issue in terms of

preservation has been the persistence of numerous cracks that have formed in the cement plaster, often times leading to a loss of ornamentation. In order to better understand the behavior of the towers, LACMA contacted the UCLA Department of Civil and Environmental Engineering in order to set up sensors on the Center Tower. Data have been collected on accelerations, wind loads, temperatures, and crack movements. The main goal of the UCLA team has been to monitor how the environment (wind, temperature, and earthquakes) affects the behavior of the tower and to aid in determining the likely cause of the cracks. Preliminary findings suggest that thermal loads play an important role in the tower's behavior. A finite element model of the Central Tower allows these temperature effects to be studied in greater depth.

Since data collection and analysis are still ongoing at the time this thesis will be submitted, it is not meant to give any final conclusions, but instead it serves as a summary of the key findings up to this point. This document is organized into 8 main sections. Following this introduction, Section 2 provides the background and history of the Watts Towers, starting with their construction, and finishing with a discussion of LACMA's current study. Section 3 will discuss the instrumentation that was used and how the data were processed in order to study the environmental effects. Section 4 presents the various effects the thermal loading has on the towers, including shifts in natural frequency, daily displacements, and daily crack movements. Section 5 discusses the effects of earthquakes and wind on the structure, based on the presently available—albeit limited—data set. Section 6 presents the findings regarding the coupled movements of the East and Center Towers, along with a brief discussion of the modal properties for the West Tower. Section 7 discusses the development of a finite element model of the Center Tower and the results of thermal loading simulations. Lastly, Section 8 summarizes a set of initial conclusions that can be gathered from the data collected thus far.

2 Background and History

2.1 Construction of the Towers

The Watts Towers are the work of one person, Simon Rodia, an Italian immigrant who moved to the United States in the early 1900s (Goldstone, 1997). Construction on the Towers began in 1921 in the Watts district of Los Angeles, on a triangular lot at the end of East 107th street. When Rodia began construction on the Towers, he was already forty-two years old and had experience working with concrete and tile as a construction worker. Rodia worked on the Towers for thirty-four years, constructing a total of 17 interconnected structures, adorned with thousands of objects. There are an estimated 11,000 pieces of broken pottery, 15,000 glazed tiles, 6,000 pieces of glass, 10,000 sea shells (Goldstone, 1997), and several other items, large and small, pressed into the mortar throughout the site. The three main towers rise high above the surrounding landscape, reaching heights of approximately 55, 97 $^{3}/_{4}$ and 99 $^{1}/_{2}$ feet. Rodia left in 1955; at that point, he was well into his 70s. He would die about 10 years later of natural causes, having never returned to visit his Towers (Goldstone, 1997).

Part of the difficulty in preserving the Towers and understanding how they behave as structures is the limited available information regarding the construction materials and methods used by Rodia. Rodia built the Towers by himself, without the use of any plans or drawings. Previous studies on the Towers—namely, the work done by the Ehrenkrantz Group (1983) and the research done by Goldstone (1997)—provide some insight into Rodia's methods. Each tower was started by digging a shallow foundation that was then filled with concrete. The steel members that made up the columns were pushed through the concrete as it was drying and into the soil below. The columns were wrapped with a wire mesh and then the mortar was pressed on

by hand. As the mortar was drying, Rodia would ornament the surface of each element with various objects. For the less critical horizontal bands, Rodia used rebar that was bent into shape using the nearby train tracks as leverage (Hale, 1957). Rodia built each structure from the ground up, without the use of ladders, scaffolding, machine tools, bolts, or welds. He would cast a new member on the ground and climb on top of his previous work in order to splice it into location.

Rodia made the base of each tower very heavy, which helps to provide resistance to overturning forces from earthquakes and windstorms. The base of the Central Tower, for example, is approximately 8 feet tall and is filled with large pieces of broken concrete (Goldstone, 1997). The base of each tower was cast as part of the surrounding patio, which further acts to resist the overturning forces. A ground penetrating radar survey of the floor slab found that the thickness varies from 2.5 to 4.25 inches, with only three small voids (LACMA Q5 Report, 2012). The few number of voids that were found are a testament to the high level of workmanship that Rodia used throughout the construction process.

Shortly after Rodia left, the city of Los Angeles declared the Towers unsafe and ordered them to be torn down. Thankfully, the Towers had already received national attention and were recognized as a work of art. This led to the creation of the Committee for Simon Rodia's Towers in Watts (CSRTW), (Goldstone, 1997). Engineers for the CSRTW analyzed the Towers and concluded that the city engineers were incorrect in their assertion that certain key members were unsafe and likely to fail. It was decided to settle the debate by performing a load test on the tallest of the three towers, the West Tower (Goldstone, 1963). If the tower could withstand the prescribed load, the city would reverse their demolition order.

2.2 Load Test

The load test was designed and carried out by Bud Goldstone, an aeronautical engineer. The West Tower was to be loaded for a full five minutes with a 10 kip horizontal force, a conservative estimation of the code-level wind forces (Goldstone, 1963). The force would be applied by a hydraulic cylinder in 1 kip increments and transferred from one main whiffletree beam to two other beams and then to four straps that were wrapped around the tower at heights of 15, 27, 39, and 51 feet. To ensure that the tower wasn't overloaded, the main whiffletree beam was designed to yield in flexure at the critical 10 kip load. This safety precaution ended up prematurely halting the test; once the 10 kip load was applied, the beam yielded after only one minute. The city was nonetheless satisfied with the results, and they removed the demolition order. Throughout the duration of the test no cement cracking or permanent deformations were observed (Goldstone, 1963). The weight of the West Tower has been estimated around 40 kips (Goldstone, 1997)—meaning that the tower was able to remain elastic with little damage under lateral forces of approximately 25% its total weight. With the safety of the towers proven, the next step was to start the process of restoration and preservation.

2.3 Previous Studies and Preservation Work

The first step in repairing the Watts Towers was simply to fill in the cracks and to attempt to waterproof the structures (Goldstone, 1997). Over time, moisture penetrated to the underlying reinforcement, causing the steel to rust. The corrosion of the steel was often blamed for the formation of the cracks (Ehrenkrantz, 1983). As the steel corrodes, it expands and pushes out on the concrete cover. The patch type repair method worked initially, but by the 1970s a series of rain and wind storms caused extensive cracking, resulting in a large amount of the ornamentation falling off and even causing a few whole pieces of the structures to fall off (Goldstone, 1997).

In 1983, the Ehrenkrantz Group was contracted to develop a preservation plan that attempted to recreate the materials and methods that Rodia himself used for construction and repair (Ehrenkrantz, 1983). As part of their report, they conducted an in depth study of the history of the Towers, material testing on samples of the mortar, and detailed hand calculations to estimate the distribution of forces and overall displacement under seismic and wind loading. The results of their study included recommendations for suitable epoxies, rust inhibitors, steel reinforcement, and mortars that could be used for repair.

Shortly after the Ehrenkrantz report was finalized, a team of engineers from ANCO conducted environmental monitoring with the same goal as the current study—that is, to find out how environmental variables affect the deterioration of the Towers. In the first phase of their study, they instrumented the East Tower with an accelerometer, a thermal sensor, a strain gage, and a displacement transducer. Data were sampled for 20 seconds each half-hour, for a period of 24 hours (ANCO, 1988). Their initial monitoring suggested a correlation between temperature and both steel strain and crack movements. As the temperature decreased, an increase was seen in steel strain and crack movements. For the second phase, the monitoring was extended to the Central Tower and the Gazebo, and the data acquisition package was updated to include a humidity sensor and a wind speed sensor. Data were sampled at 50 Hz for one second each hour, for a period of 99 hours. Results of the second phase were similar to the first phase and showed an inverse correlation between the movement of a crack along a column on the Center Tower and the temperature (ANCO, 1989). The Ehrenkrantz and ANCO studies provided invaluable information for early interventions on the Towers, but they were limited by the technology of the time. Modern sensor and data acquisition technology allows the same type of data to be recorded but with increased precision and for a much longer duration.

2.4 Current Preservation Efforts

After almost three decades with the Ehrenkrantz conservation handbook serving as the key reference document for repairs on the Watts Towers, an updated procedure was long overdue. In 2011, the Los Angeles County Museum of Art partnered with City of Los Angeles' Department of Cultural Affairs with the objective of revising the Ehrenkrantz report and developing a new comprehensive long-term preservation plan.

One of the first steps in LACMA's work was to organize and digitize the vast amount of information that exists on the Towers such as previous work orders, test results, photographs, etc. As part of the organizational effort, the existing documentation regarding conservation and repair work was reviewed in order to determine which methods had been successful, and which ones had not. The goal was to determine the effectiveness of each intervention method and to estimate the rate of deterioration of the Towers. The main goal of the project is the same as previous efforts—to repair and preserve the Watts Towers. This is accomplished by determining the most efficient elastomeric crack fillers, finding means to secure loose ornaments, determining compatible mortar mixes for larger repairs, and waterproofing the structures to prevent further oxidation (LACMA Quarterly Reports, 2011-13). For the said goal, the LACMA conservators find it necessary to better understand all the factors contributing to the deterioration and to understand the reasons underlying the failure of past interventions. At the request of the LACMA conservation team led by Dr. Frank Preusser, the current study has been focusing on analyzing the global structural behavior of the Watts Towers, including collection of data on structural response (accelerations and crack displacements) and environmental loads (temperature, wind speed, wind direction). The data will be analyzed to determine how the environmental loads affect the behavior of the tower and the movement of cracks. The environmental monitoring will

be coupled with the development of a detailed finite element model. The FEM model will be used to look at the steady-state displacements and stress distributions during thermal loading in order to determine whether these stresses may be a possible cause of crack formation and propagation.

3 Instrumentation

In order to analyze the behavior of the Central Tower, a monitoring system was installed on the tower, which included accelerometers, inclinometers, displacement sensors, dynamic wind sensors, and temperature sensors.

Accelerometers were used in order to record ambient, earthquake, and wind induced vibrations. The accelerometers were all EpiSensor ES-T models, designed and produced by Kinemetrics (Kinemetrics, 2008). The triaxial EpiSensor force-balance accelerometers have a flat frequency response between 0-200 Hz and can measure acceleration amplitudes from below 1 μg to a 4g clip level. One accelerometer was attached to an intermediate column on the north side of the Central Tower, approximately 23 feet above the ground. An additional accelerometer was placed on the ground, 90 feet to the west of the Center Tower.

An inclinometer was used to track the motion of the tower. This device is a precision biaxial tiltmeter (model 716-2B) from Applied Geomechanics (Applied Geomechanics, 2001), which is accurate down to approximately 1 μrad. The tiltmeter was attached at the same location on the tower as the accelerometer. This sensor also includes an internal thermometer that was used for the initial stages as an estimate of the ambient and surface temperatures.

Figure 3.1: Location of the accelerometer and the tilt meter

In order to directly measure the crack movements, two cable-position transducers, Model 150 from Firstmark Controls (Firstmark Controls, 2013), were placed over existing cracks, transverse to the direction of crack propagation. Unlike traditional string potentiometers that are primarily used for static or quasi-static displacement readings, the design of this sensor allows it to capture small amplitude static and dynamic displacements with a resolution of <1 μinch. The crack sensors provide data on how the cracks open and close over the course of the day, whether or not the crack is continuing to open over time, and what effects, if any, earthquakes and wind have on the crack movement.

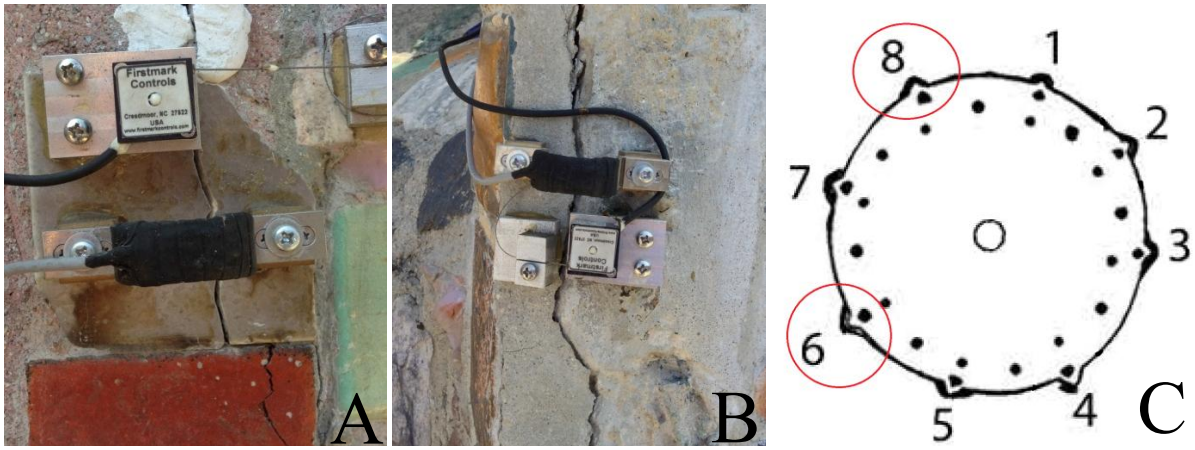

Figure 3.2: (A) North and (B) south side crack displacement sensors (C) location of sensors

Dynamic wind speed, wind direction, and air temperature were recorded using an ultrasonic anemometer, Model WindObserver 65 by Gill Instruments (Gill Instruments, 2013). The sensor was mounted approximately 10 feet off of the north side of the Central Tower and 15 feet above the ground surface. This positioning allows the sensor to get a clean reading, free from most of the turbulent zones created by the towers or the surrounding walls. The sensor was placed on the north side of the tower because the strongest winds at the site are from the Santa Ana winds. The Santa Anas are strong, seasonal, and persistent downslope winds that blow

northerly at the site. This sensor can measure dynamic components of wind gusts to about 5 Hz, and so will be a proxy for dynamic wind pressure on the Central Tower.

Figure 3.3: Wind sensor

The sensors were all connected to Quanterra Q330 data-loggers (Quanterra, 2013). The Q330 features high-resolution 24-bit A/D conversion and GPS time stamping that is accurate down to a microsecond. Each Q330 has only six channels of input, but the GPS time stamping allows for synchronization across multiple digitizers. Data were sampled continuously at 200 Hz. Real-time data were gathered by an on-site computer running Kinemetrics Rockhound software. Data from all sensors were recorded continuously and saved to a new output file at the beginning of each hour.

In addition to the sensors mentioned above, LACMA previously installed a weather station on top of a storage trailer located at the northwest corner of the site and crack displacement sensors at three different locations on the Central Tower. The LACMA weather station records additional variables such as humidity and solar radiation, which help to better understand the environmental conditions.

The UCLA sensors were deployed in different phases, with new sensors being added as they became available or were deemed necessary. The first phase consisted of only the

accelerometer and the tiltmeter and lasted from January 30 to March 11, 2013. Phase two added the two crack displacement sensors and the wind sensor. Although the crack sensors were installed on March 11, they were initially using the Q330 as a power supply, which introduced undesirable amounts of noise into the data. It wasn't until they were hooked up to a custom low-noise voltage reference on April 8 that the crack displacement data were considered usable for measuring the small daily movements. The third phase started on May 10 when the tiltmeter was removed and the ground accelerometer was added. Data collection using this sensor arrangement is still continuing at the time this thesis is submitted.

During the week of July 29, additional sensor arrangements were completed with the help of an articulated boom truck, which allowed sensors to be placed at previously unreachable heights. The first arrangement consisted of placing two accelerometers on the Central Tower at heights of 45 and 53 feet, one accelerometer on the East Tower at 33 feet, and one accelerometer on the West Tower at 34 feet. A second arrangement was completed with all four of the new accelerometers on the Central Tower at heights of approximately 10.5, 31, 45, and 53 feet.

3.1 Data Acquisition and Processing

As part of the California Strong Motion Instrumentation Program (CSMIP), the California Geological Survey (CGS) has published system requirements for the use of accelerometers. They specify a minimum ADC resolution of 18 bits and a sampling rate of 200 Hz (CGS, 2007). Results of a series of digital simulations and sensitivity analyses show that a minimum sampling rate of 200 Hz and an effective resolution of 8 bits/g (approximately a 12-bit ADC resolution over $\pm 4g$) limits the error in the recorded accelerations to less than 5% (Skolnik, 2008). The choice to use a 24-bit ADC system with a 200 Hz sampling rate for the Watts Towers monitoring

was based on this knowledge and the desire to accurately capture short-term dynamic motions of the tower with a wide range of amplitudes from ambient to earthquake.

A main goal of the project is the analysis of long-term behavior of the tower; to this end, analyzing the full data set of 200 samples per second is unnecessary. In order to study the response of the tower to the environment, the tilt, temperature, and crack displacement data were all averaged within each one-hour block. The tilt and crack data were further processed in order to normalize their baseline values to zero.

A number of different times the data acquisition system would momentarily stop recording, leading to a small loss of data. The amount of data lost typically corresponded to a window of less than 5-10 minutes. For these small loses in data, the remaining data in the one-hour block were averaged, and no gap in the time-history was assumed. In a couple of cases, the amount of data lost was on the order of several hours to a few days due to power loss at the site. These events are presented as a gap in the time-history plots.

4 Thermal Effects

The Watts Towers site is located in East Los Angeles, an area where temperatures can often be relatively high compared to the more temperate coastal areas of West Los Angeles. The LACMA weather station recorded an average peak daily temperature of 26.7°C and a high of 38.7°C during summer 2012. Even for a relatively mild air temperature of around 24°C, the surface temperature of elements exposed to the sun has been shown to exceed 49°C (LACMA Q6 Report, 2012). These high temperatures have several effects on the Towers.

4.1 Comparison of LACMA and UCLA Weather Data

The LACMA and UCLA weather data will both be used to examine various trends, so it is necessary to check how they compare to each other and to verify that the recorded values for temperature and wind speed are consistent. The LACMA station samples the weather data once every five minutes. To facilitate a one to one comparison, the UCLA data were resampled at the five-minute rate.

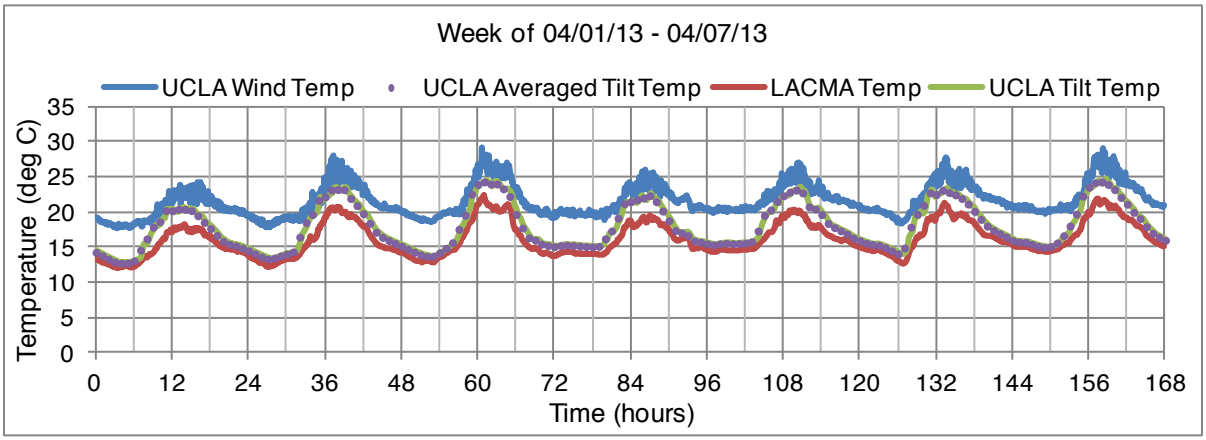

Figure 4.1: LACMA vs. UCLA temperature comparison

The highest temperature values come from the wind sensor, followed by the tiltmeter, with the LACMA station reading the lowest values. On average, the tiltmeter and the wind sensor

record 1.7°C and 5.4°C higher temperature values than the LACMA station, respectively. Another thing to note is that the one-hour average temperature values follow the same trend as the 5-minute sampling—accurately capturing the peaks and valleys throughout the day. The tiltmeter and LACMA weather station are within a close enough range that the difference can likely be attributed to variations in exposure and location. The temperature difference between the wind sensor and the other two sensors is large enough that it will have to be taken into consideration when using the data.

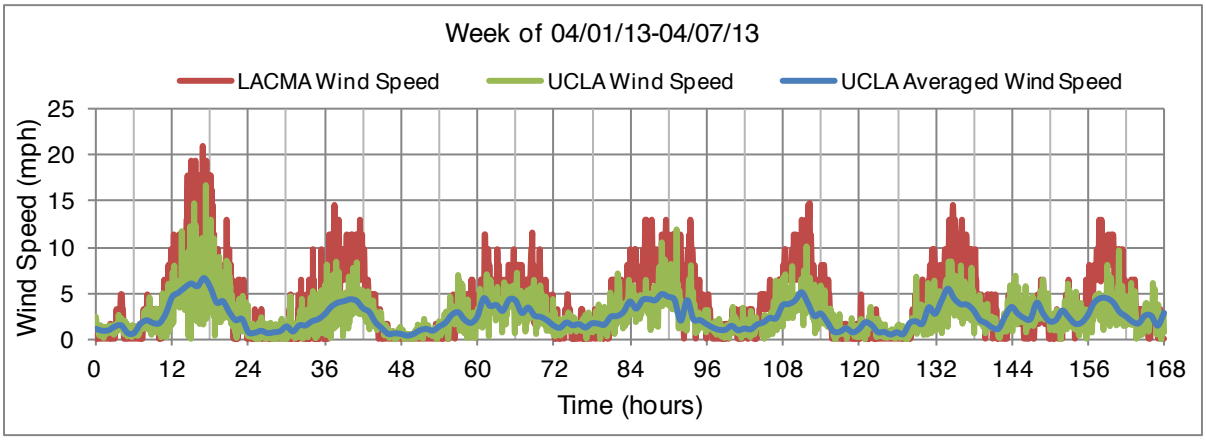

Figure 4.2: LACMA vs. UCLA wind speed comparison

Opposite of the temperature data, the LACMA weather station recorded higher values for wind speed than the sensor attached off of the tower. The wind speed recorded by the UCLA sensor was 1.4 mph less, on average, than the LACMA station. Again, this difference is small and likely due to the LACMA station and UCLA sensor being located at different heights with different exposures. Taking a one-hour average of the wind speeds leads to a large decrease in the peak values, which is not surprising considering peak wind speeds are registered as gusts during relatively short periods of time. When looking at a full hour, the gusts are averaged with periods of low wind speeds, thus reducing the value. Even the five-minute sampling rate leads to an underestimation of peak speeds. For example, at hour 18 (6 pm on 4/01) the five-minute data give a peak value of 15 mph, whereas the actual peak wind gust was around 23 mph. These data

nonetheless tell the story of when wind speeds peaked, and the full data set can be analyzed during periods with strong gusts in order to determine any short-term responses.

4.2 Effect of Temperature on Fundamental Frequency

The frequency of a structure is an important parameter as it provides an estimate of the structure's global stiffness. The first three frequencies of the Central Tower can be easily identified by finding the averaged power spectral density (PSD) of the acceleration signal. The function `pwelch` was used in Matlab, which returns the estimated PSD using Welch's averaged modified periodogram method (MATLAB, 2013). Welch's method involves breaking a record down into a set of possibly overlapping segments, finding the periodogram of each segment by computing the discrete Fourier transform, and then averaging all of the periodograms together (Welch, 1968). When looking at a finite sample size, anomalies in the estimated spectra may occur due to spectral leakage (Bendat & Piersol, 1993), which occurs due to the presence of signals that are non-periodic within each data segment and therefore lead to discontinuities at the boundaries (Harris, 1978). Weighting functions, called windows, can be used to taper the data within each segment and reduce the effects of spectral leakage. The function `pwelch` defaults to dividing the signal into 8 segments with a 50% overlap (Matlab, 2013). Increasing the number of segments to be averaged together helps to reduce the variance in the estimated spectrum. Therefore, in this case, the segment size was set to 20,000 data points while using the same 50% overlap, resulting in 71 different segments for one hour of data. A Hanning window was specified in order to smooth the data within each segment. Increasing the number of segments may lead to an increase in accuracy, but it also causes a drop in the frequency resolution. The choice of 20,000 data points per segment results in a frequency resolution of 0.01 Hz, which was determined to be high enough for the purposes of this study.

By plotting the resulting power density versus frequency, it is easy to identify the first three modes, as shown in Figure 4.3. The simple method of "peak-picking" was used here to obtain the dominant natural frequencies (cf. circled locations in the figure). In order to pick the peaks, a range of frequencies was selected for each mode after viewing the initial results. For example, the first mode was assumed to fall between 1 and 3 Hz, the second mode between 3 and 5 Hz, and the third mode between 5 and 8 Hz. The maximum value was found within each of those ranges, and the corresponding frequency value was saved. There are other, more advanced, methods that can be used to identify the dominant modes, but the simplicity of peak-picking and the ability to automate the process in Matlab made it the preferable option when dealing with such a large data set.

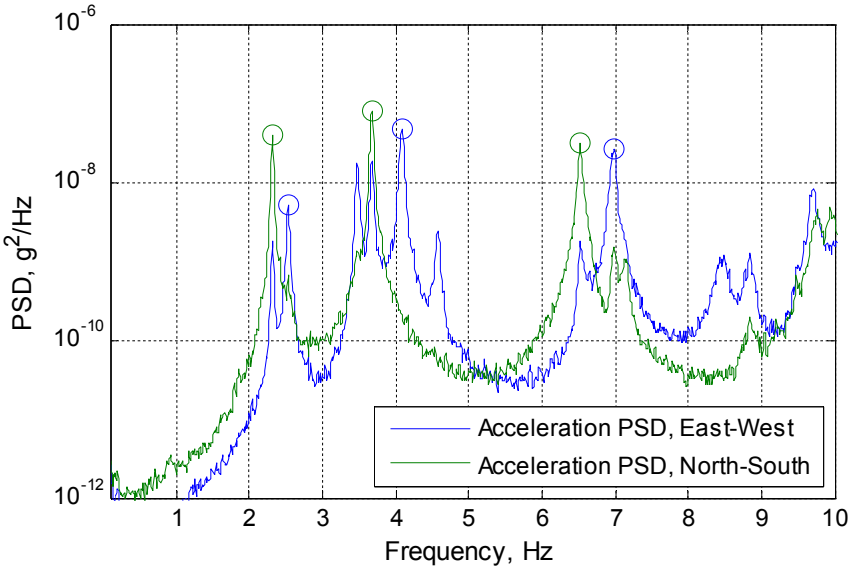

Figure 4.3: Acceleration power spectral density

The East and Central Towers are coupled together by a series of connecting beams. This coupling leads to a complex PSD signal in the east-west direction. The first three frequencies in the east-west direction are all larger, showing that the tower is stiffer in that direction than it is in the north-south direction. Since the Central Tower is approximately symmetrical, the increased stiffness is also likely due to the coupling of the two towers. This coupling effect is discussed in

greater depth in §6. The dominant frequencies were identified for each one-hour set of data using the previous methods. Figure 4.4 displays the shift in the north-south first mode frequency relative to the variations in temperature during the first week of February.

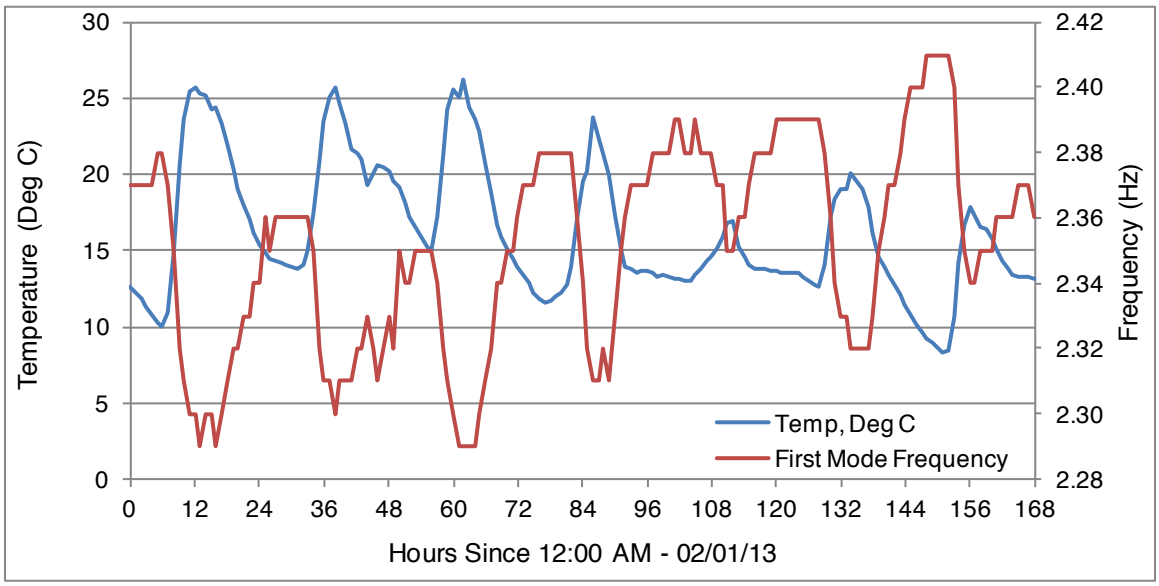

Figure 4.4: Frequency vs. temperature over time

A clear trend can be seen in this figure; as the temperature increases, the stiffness of the tower decreases, causing a drop in first mode frequency. The Central Tower acts as an unrestrained cantilever; as the temperature increases, the structure expands and the material becomes more flexible. It was found that throughout the day, the first mode frequency in the north-south direction could vary by as much as 5%; over the course of several days, the variation is as high as 8%. The shift in higher mode frequencies was even larger, with long-term variations of approximately 12% for the second and third modes in the north-south direction. The first mode frequency of a structure is proportional to the square root of its stiffness and inversely proportional to the square root of its mass. The mass of the structure will change slightly over time due to variations in moisture content on wet or dry days, but overall the differences will be negligible. The mass can therefore be considered constant, meaning an 8% shift in frequency corresponds to approximately a 15% shift in stiffness. The change in frequency can be seen over

the course of several months through the figures below, which show the hourly variation in frequency between January 30, 2013 and May 12, 2013.

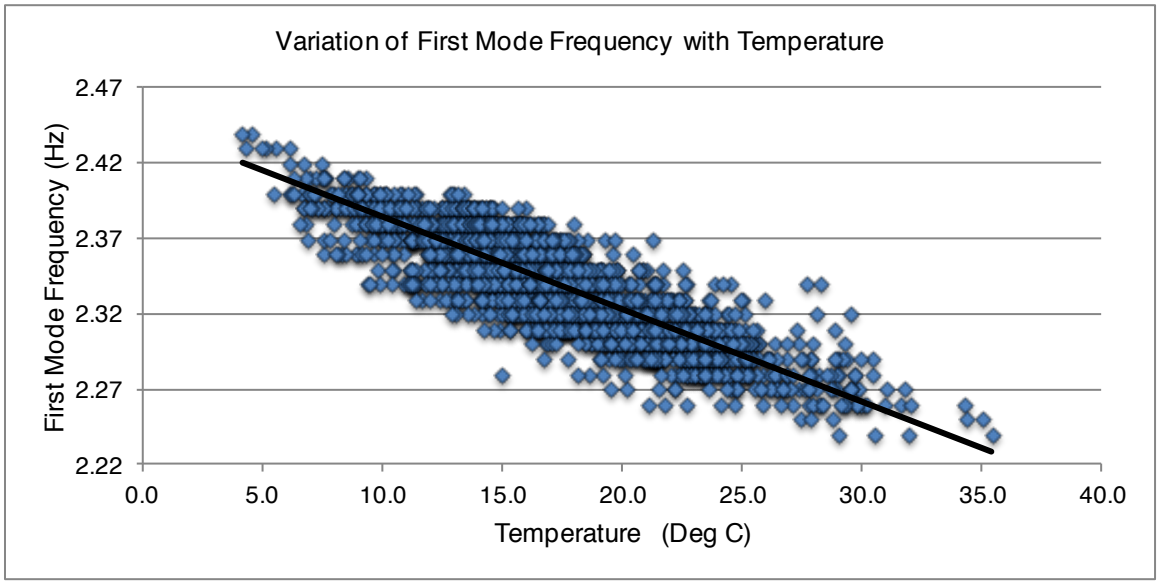

Figure 4.5: January - May frequency vs. temperature

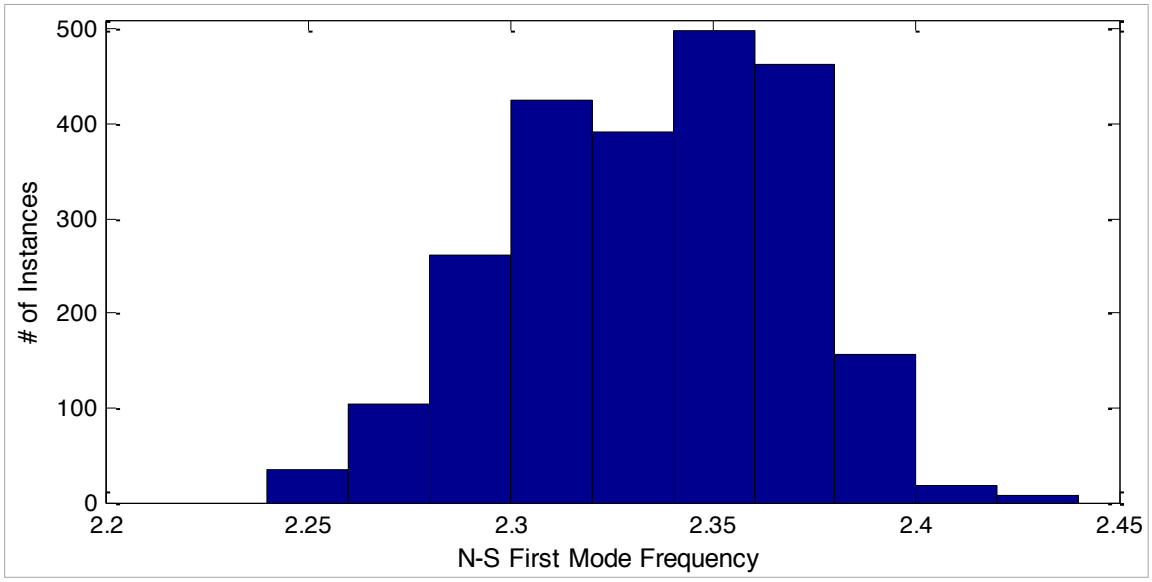

Figure 4.6: Frequency histogram

This daily shift in frequency has been noticed before in other types of structures. During a study of the Alamosa Canyon Bridge, a seven-span bridge in southern New Mexico, it was noted that the first-mode frequency of the bridge varied by around 5% each day (Farrar et al., 1997). A simple test structure with steel HSS columns supporting a concrete top slab was shown to have a

daily fluctuation of 10% when the structure was braced laterally with HSS cross-braces and a 3% daily fluctuation when it was in an unbraced condition (Asghari, 2009). The frequency of this system was also shown to vary based on other environmental parameters such as the location of the water table and the amount of soil saturation. Over time, the softening of materials can have a large effect on a structure's frequency. The dynamic properties of the Robert A. Millikan Library on the campus of the California Institute of Technology (Caltech) have been studied since shortly after its construction. Since 1967, the baseline fundamental frequency has shifted down by 22% and 12% in the east-west and north-south directions, respectively (Clinton et al., 2006).

An important implication of this shift in frequency is from a structural health-monitoring standpoint. In structural health-monitoring studies, the frequency is often calculated before and after an event, for example an earthquake or wind storm, with the anticipation that any damage to key structural members will cause cracking and/or loosening of connections, which will result in a lower stiffness. If the frequency of a structure is significantly lower following an event, then it is likely that there has been some damage. Difficulties may arise, however, due to the fact that not all forms of damage will cause large shifts in the lower mode frequencies. Local response such as damage is typically captured by higher frequency modes, and the energy necessary to excite these modes is higher (Doebling et al., 1998). Therefore, the shifts may not always be visible under ambient vibrations. This means that the effects of temperature and other environmental variables can mask any damage induced shift in frequency. Farrar et al. (1999) recommend a method of normalizing the response output by the environmental input. This method effectively minimizes the influence of environmental or operational variability in order to better distinguish changes in the system. Various statistical pattern recognition methodologies

can then be used on the data to determine if a noticed shift in behavior is in fact significant and therefore a likely indicator of damage (Farrar et al., 1999).

The process of identifying damage can be broken into four levels (Rytter, 1993).

- Level 1: Determination that damage is present in the structure
- Level 2: Level 1 plus determination of the location of the damage
- Level 3: Level 2 plus quantification of the severity of the damage
- Level 4: Level 3 plus prediction of the remaining service life of the structure

The previously mentioned statistical damage detection algorithms typically can only identify Level 1 or Level 2. Level 2 damage detection requires either a large amount of sensors, to study the changes in the mode shape, or an energy input that is capable of exciting the higher modes (Farrar et al., 1999). When an accurate finite element model of the structure exists, a set of possible damage scenarios can be assumed and modeled. The observed shifts in dynamic behavior can then be compared to the changes in the model behavior. For a given damage scenario, if the shift in the model is similar to the observed shift, then it is possible that type of damage has occurred. Friswell et al. (1994), and Hemez and Farhat (1995) discuss methods of using finite element models for damage detection.

Even for low-level ambient vibrations, the power spectral density of the acceleration signal clearly shows the first few modes of vibration for the Central Tower. The data recorded during the monitoring period can serve as a baseline set that can later be compared to new recordings in order to see if there is any decrease in stiffness over time due to material softening, or if there has been a change in stiffness following an earthquake or windstorm. The length of the data set, spanning over multiple seasons, tells a clear story of how temperature affects the fundamental frequencies. This defined relationship can be removed from the data set in order to better

distinguish shifts in the system. With a calibrated finite element model of the Central Tower also available, it is possible to further study local damage effects for a better idea of how damage may affect the global behavior.

4.3 Daily Tilt Cycles

Plants will grow toward a light source in order to maximize the amount of energy available for photosynthesis—a behavior known as phototropism. The Central Tower conversely leans away from the sun over the course of the day due to differential heating of the side exposed to the sun compared to the shaded, cool side. The elements on the sunny side will expand faster and to a larger extent. The figure below displays the daily tilt cycles in the north-south and east-west directions.

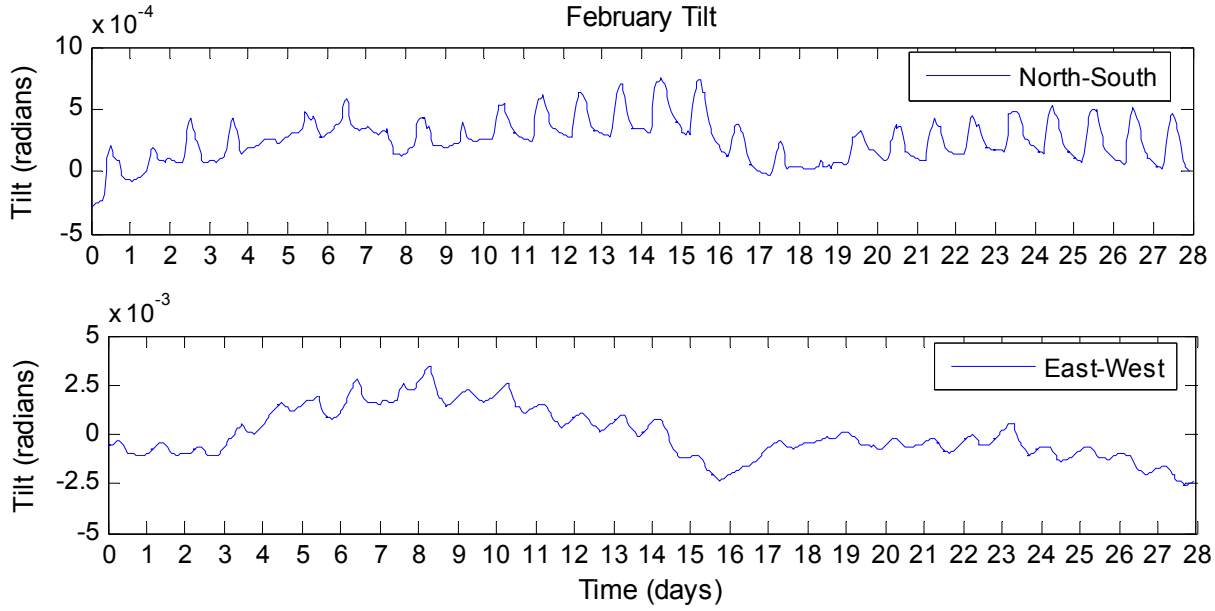

Figure 4.7: Thermally induced daily tilt cycles

In the N-S direction, the daily variation is around 4×10^{-4} radians, whereas in the E-W direction, the daily variation is larger—around 9×10^{-4} radians. It is not known at this time why the tilt is larger in the E-W direction as compared to the N-S direction. The tilt data can be used

to estimate the tip displacement using a few different approximations. The simplest method is to assume uniform rotation over the height of the tower, in which case the displacement can be found by simple geometry, as in:

$$\Delta_{tip} = H_{tip} \times \tan(\theta_{sensor}) \approx H_{tip} \times \theta_{sensor} \qquad (4.1)$$

Note that θ must be in radians to use the small angle approximation of $\tan(\theta) \approx \theta$ in the equation above. Using this approximation and a total height of 97.75 feet, the estimated daily tip displacement is slightly greater than 1 inch in the E-W direction and slightly less than 1/2 inches in the N-S direction. A more advanced method would be to approximate the tower as a uniformly loaded cantilever beam, which would result in the following displacement pattern.

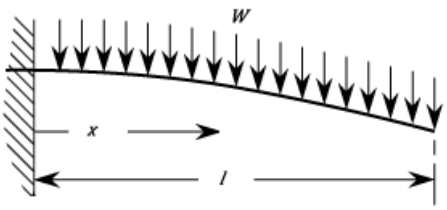

Figure 4.8: Uniformly loaded cantilever displacement pattern

The rotation and displacement at any point along the beam can be calculated as (Hibbeler, 2008):

$$\theta(x) = \frac{-w}{6EI}(x^3 - 3lx^2 + 3l^2x)\,, \Delta(x) = \frac{-w}{24EI}(x^4 - 4lx^3 + 6l^2x^2)\,,\ \Delta_{tip} = \frac{wl^4}{8EI} \qquad (4.2 - 4.4)$$

where x is the location along the beam, l is the total length, w is the magnitude of the loading, E is the Young's modulus, and I is the second-moment of the cross-sectional area. The value for rotation is known at the location of the sensor, x = 23 feet. Plugging in this value along with a total length of l = 97.75 feet, and then taking the ratio of displacement to rotation, allows the tip displacement to be estimated as follows:

$$\Delta_{tip} = \theta_{sensor} \times \frac{-6(97.75^4)}{8[23^3 - 3(97.75)(23)^2 + 3(97.75)^2(23)]} = -132.6 \times \theta_{sensor} \qquad (4.5)$$

Equation 4.5 is valid when θ is in radians and the resulting displacement is in feet. This method estimates the daily displacement at 1.43 inches in the E-W direction and 0.64 inches in the N-S direction. E and I were assumed to be constant over the height of the tower, thus their values cancelled out when finding the relationship between rotation and displacement. This method will likely underestimate the tip displacement, because the stiffness of the tower decreases significantly along its height as its peripheral columns all move closer to the center. These approximations will later be compared to the results of a computer model in §7.

In both directions, there is a noticeable long-period drift to the tilt data. These trends may be a function of electronic drift or might reflect real behavior. The values tend to return to zero, however, which suggests that it is an actual behavior of the tower. One possible explanation is that during abnormally hot days, the tower tilts to a more extreme angle, and during the night it does not fully return to its initial position before the next daily cycle. Figure 4.9 displays the average daily temperature versus the peak daily tilt for the month of February.

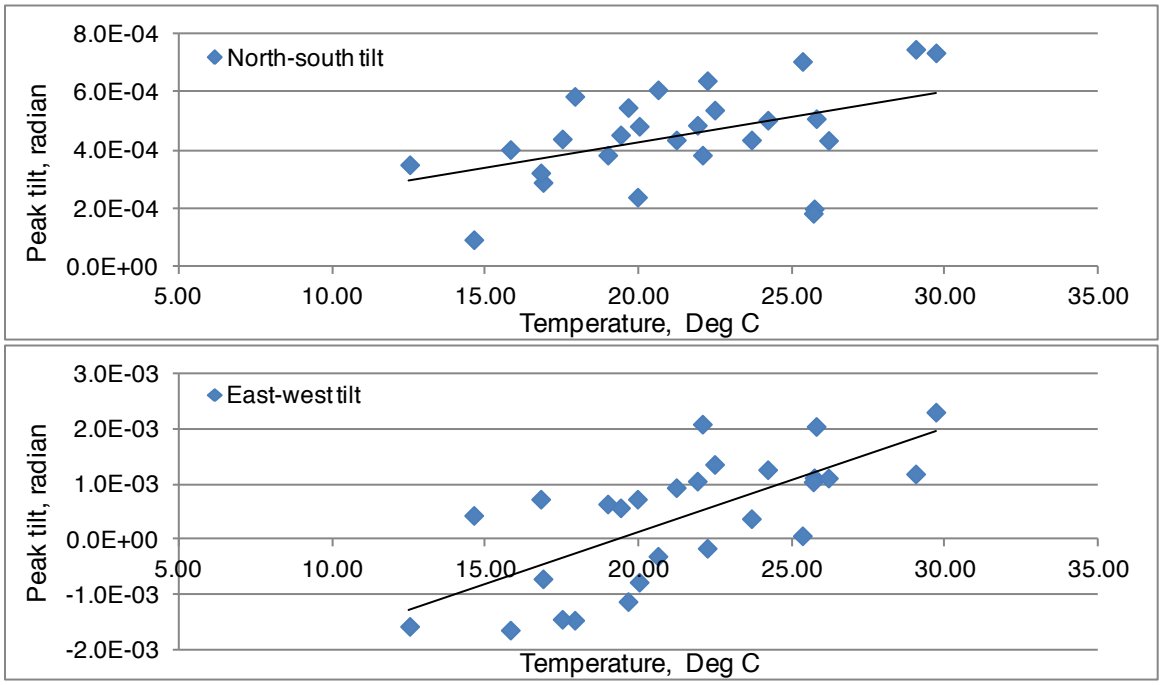

Figure 4.9: Average daily temperature versus peak daily tilt

The temperature and tilt tend to follow a similar pattern; an increase in temperature leads to an increase in the peak tilt, which suggests that this hypothesis is credible. The relationship appears to be stronger in the E-W direction than it is in the N-S direction. Other transient factors such as windstorms can influence the tilting behavior of the tower. In order to better visualize the daily motion of the tower, the data were filtered using a fifth-order Butterworth band-pass filter, which is available in Matlab's signal processing toolbox (Matlab, 2013). The low-pass frequency was set at 1/30 [1/hr], and the high-pass frequency was set at 1/18 [1/hr]. This filtering effectively leaves only the 24-hour period data.

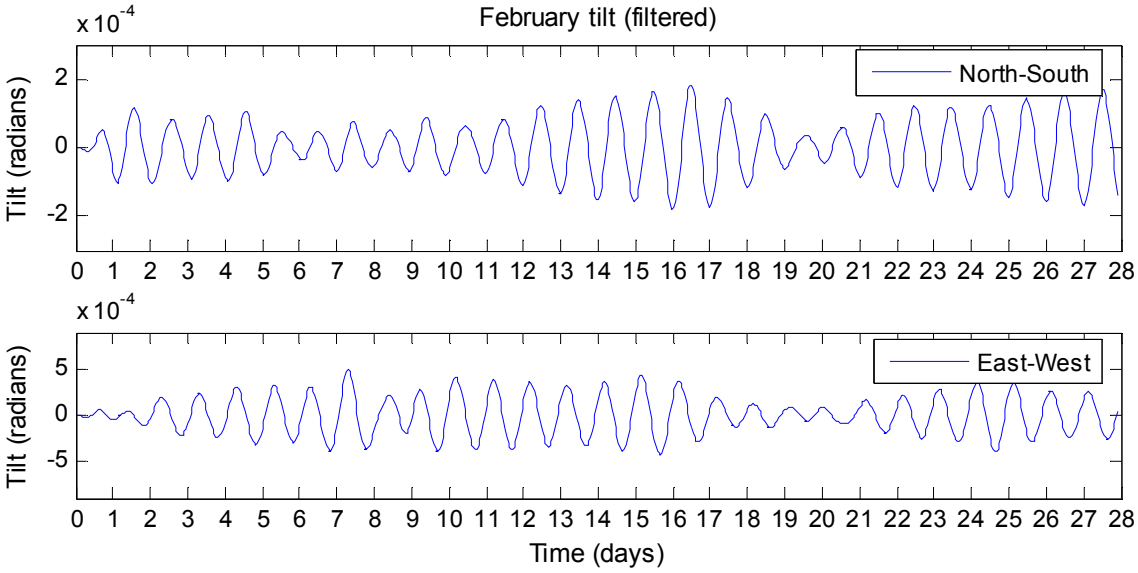

Figure 4.10: Band-pass filtered February tilt

It was hypothesized that the tilting behavior of the structure is governed by the direction of incoming sunlight. In order to estimate the location of the sun, the Matlab file `SolarAzEl.m` was downloaded from the Matlab file exchange (Matlab, 2009). With the site coordinates (latitude, longitude, and elevation) and time of day as inputs, the program calculates the approximate position of the sun, reported as an azimuth angle (position in the horizontal plane relative to north) and an elevation angle (position in the vertical plane relative to the ground

surface). Plotting the azimuth angle versus the resultant tilt of the structure allows the hypothesis to be tested.

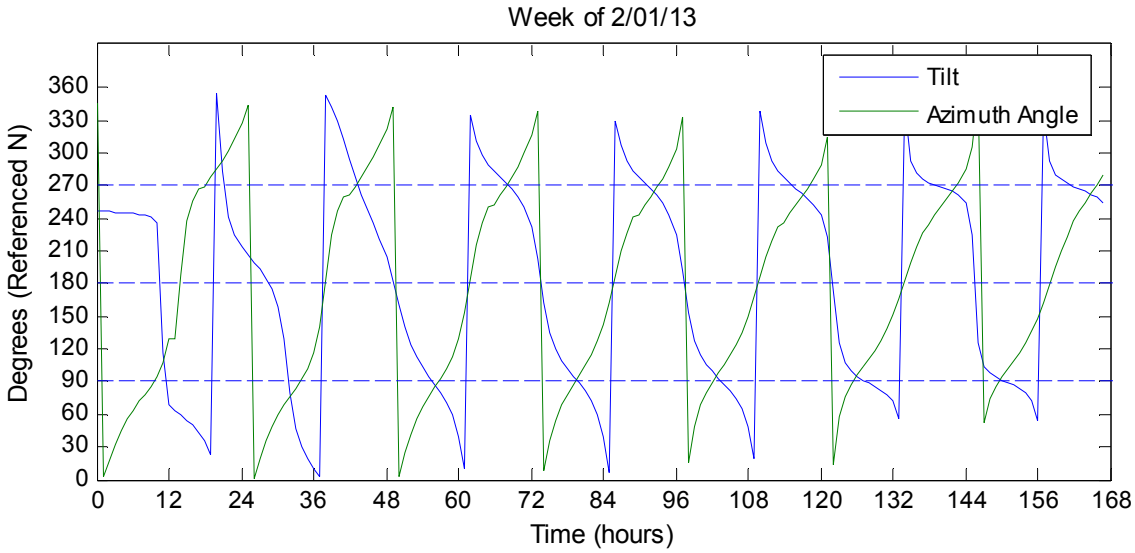

Figure 4.11: Week of 2/01/13 tilt versus the azimuth angle

The tower's motion does in fact correlate very well with the azimuth angle. There are three times of day to note in the above figure. At sunrise (~7 am), both the tilt and azimuth are approximately due east. The same behavior is seen at sunset (~8 pm) when the tilt and azimuth are in the west. In the middle of the day, however, the sun is located to the south, and the tower is directly opposite, leaning toward the north. The daily cycle is then, the tower and sun "meet" at sunrise in the east. The tower moves counterclockwise toward the north as the sun's position moves in a clockwise direction toward the south. At noon, the tower is at its most northern point, whereas the sun is at its most southern point. They continue to move until the sun and tower both reach the west. At this point the sun sets, and the tower continues its counterclockwise rotation toward the east, where it is again met by the sun the following day. This behavior suggests a time lag between when the sun is hitting a certain part of the tower and when it starts to lean away. This circular behavior is clearly seen in the next set of plots, which show the track of the tower throughout the month of February, and the location of the tower at the previously noted three

times of the day. Note that the sunrise and sunset times are approximated in these figures. The magnitude of displacement is based off the uniform rotation approximation.

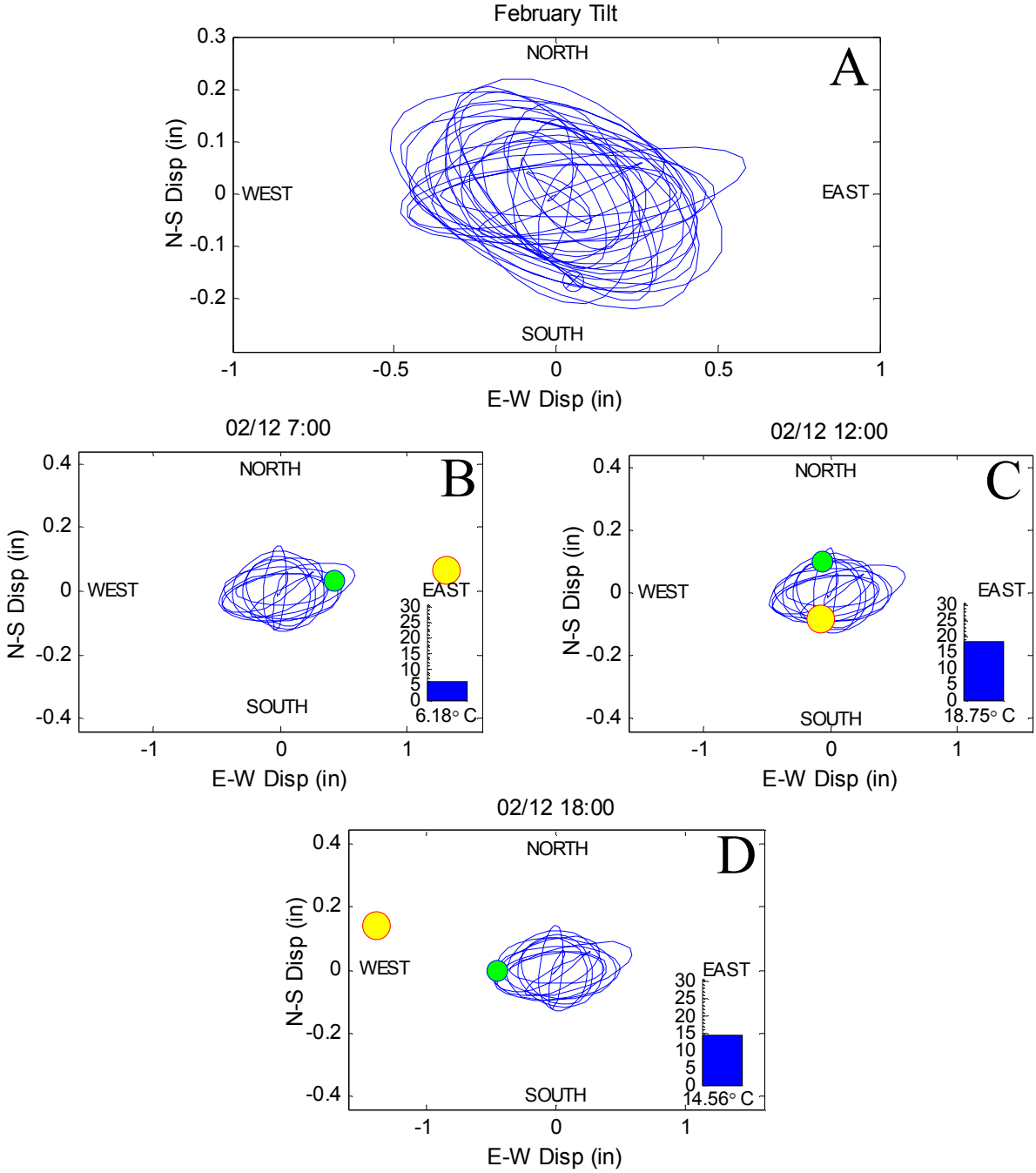

Figure 4.12: Daily tilt cycles (A) month of February (B) sunrise (C) noon (D) sunset

Solar heating will introduce stresses into the tower's members due to local expansion. It is also possible that this global tilting behavior will add additional stresses into the members as the tower moves around over the course of the day. The displacement and stress patterns will be studied again as part of the computer modeling in §7.

4.4 Crack Displacement

The ultimate goal of this study is to aid in the preservation of the Towers. One of the key components in the restoration process for LACMA is to repair existing cracks and ideally discover methods to prevent the formation of new cracks. In order to accomplish this, it is necessary to understand how the cracks are behaving. Two cracks were selected along the base of the Central Tower's exterior columns as shown previously in Figure 3.2. These two cracks are representative of a common type of crack that has formed on the various different parts of the structures.

The cracks along the Central Tower's columns were also instrumented by the LACMA team with two different types of sensors. On the north column, LACMA placed a TML PI-2 displacement transducer, which works by attaching a combination of strain gauges across an arch-shaped spring plate. The south column was instrumented with another PI-2 sensor, as well as a UB-5A displacement transducer. Mounting of the UB-5A transducer requires cutting into the column around the crack, whereas the PI-2 is surface mounted with epoxy, making the PI-2 the more desirable option. Figure 4.13 shows the north and south crack displacement as recorded by both the UCLA and LACMA systems.

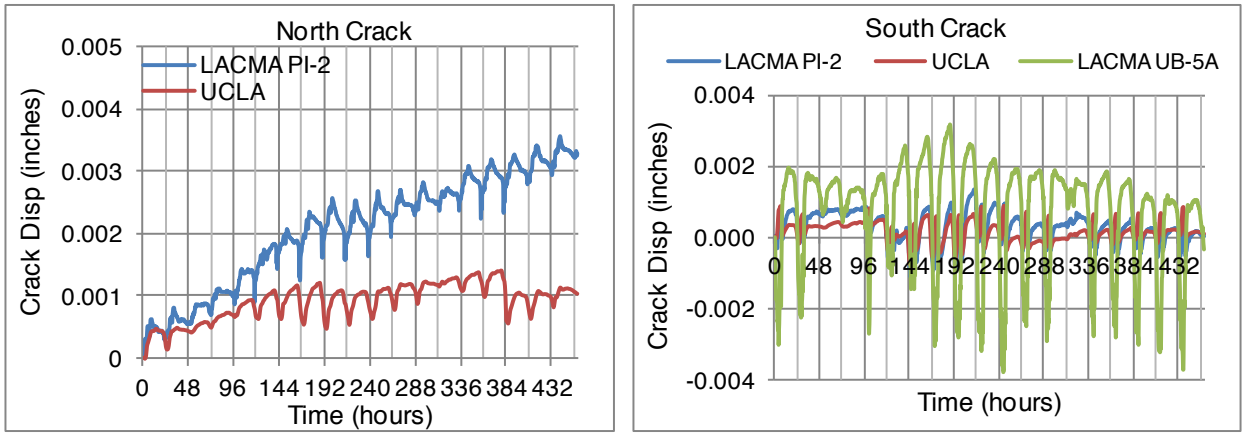

Figure 4.13: LACMA vs. UCLA crack displacement comparison

The first thing to note in Figure 4.13 is that the north crack appears to be drifting off of its baseline. The amount of drift is larger for the LACMA sensor, but since this long-term movement is observed by independent sensors, it is likely that this suggests a gradual opening of the crack and not an electronic drift in the signal. The south crack, on the other hand, displays a more widely variable behavior; yet over time, it tends to remain around a set baseline. Comparing the two systems, the LACMA PI-2 sensors seem to agree well with the UCLA sensors in regards to the magnitude of crack movement. The LACMA UB-5A sensor is recording much larger displacements, which likely are not correct. It is possible that micro-cracks formed in the column during the installation of the UB-5A sensor, causing the erroneous displacement behavior.

The long-term drift in the north crack continued for a period of time before leveling off. Figure 4.14 shows the north crack's displacement for the first four months of monitoring, between April 13 and August 13, 2013. During the first five weeks, the crack opens approximately 0.003 inches, much larger than the average daily opening and closing. The downward spike at the beginning of the sixth week is likely due to some form of work being done on or around that column. The crack remains fairly close to its baseline for the remainder of the time.

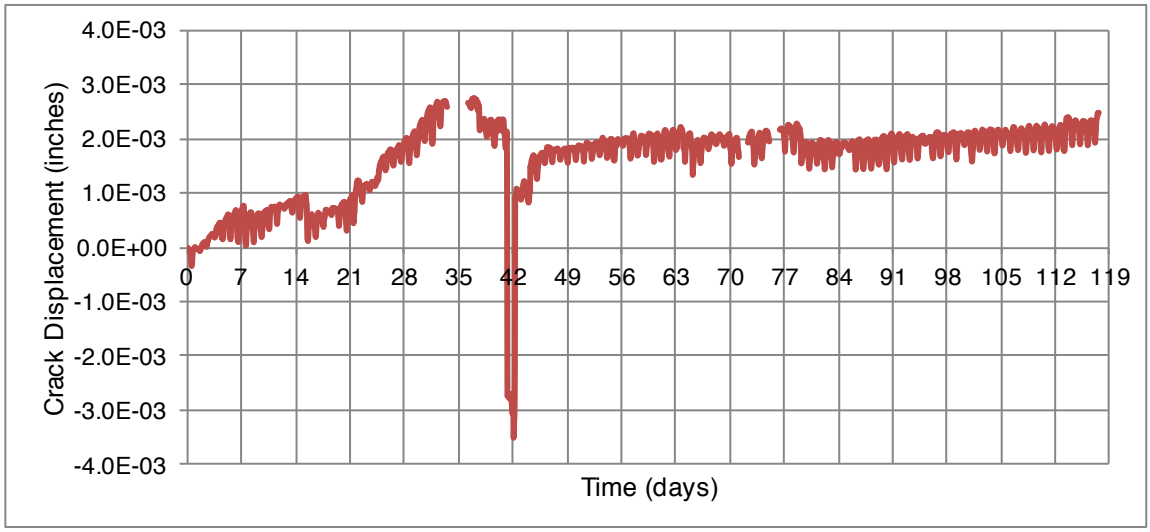

Figure 4.14: North crack displacement time-history

On a daily basis, both cracks display remarkably consistent, albeit distinct, behaviors, as shown in Figure 4.15 on the next page. The north crack follows an inverse relationship with temperature. As the temperature increases, the crack tends to close. This is likely due to the concrete cover expanding. The south crack, on the other hand, has a bimodal shape that bottoms out around noon each day, before opening back up until around 4-6 pm. At sunset, the crack starts to close again. The daily displacement for the north crack is around 0.0004 inches, whereas the south crack is more active with a larger daily displacement of 0.001 inches.

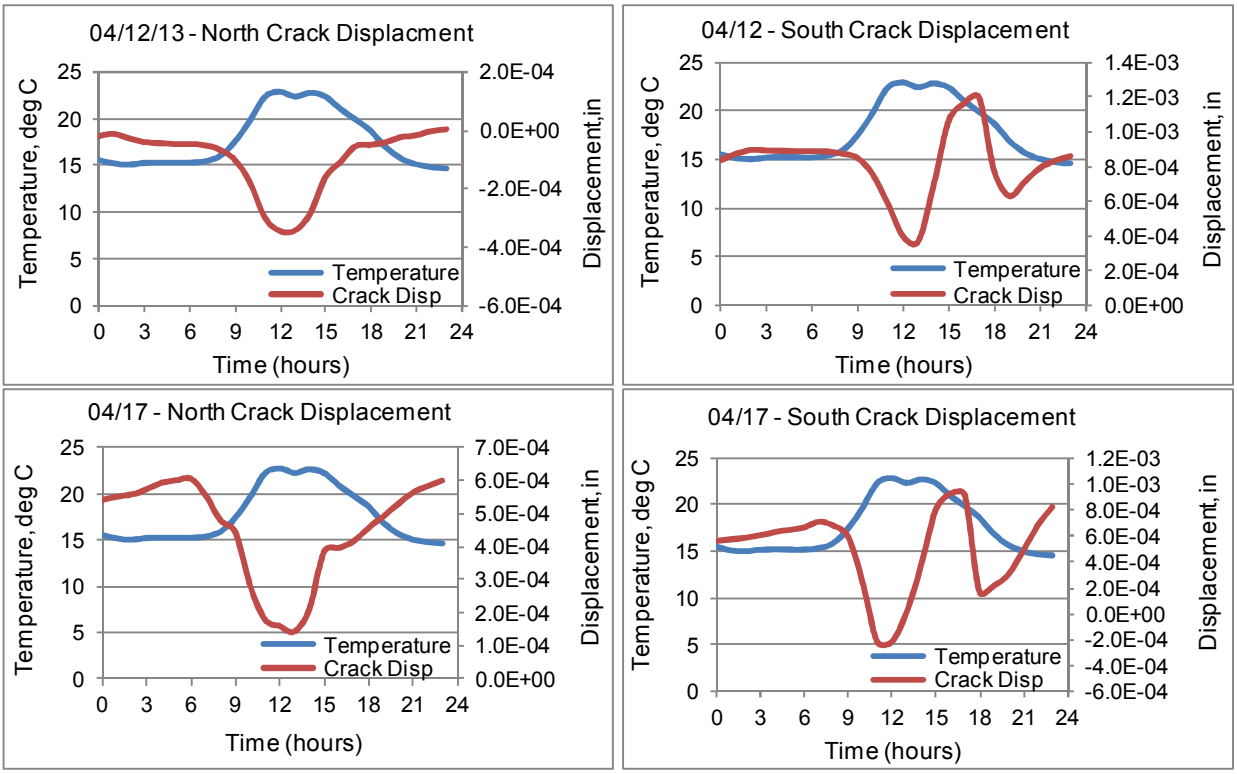

Figure 4.15: North and south crack daily displacement for 4/12 and 4/17

Throughout the day, the north crack remains in the shade, while the south crack is exposed to direct sunlight. It was hypothesized that this direct exposure to sunlight may explain not only the difference in magnitude between the two cracks, but also the difference in their behaviors. Following this logic, on a day when there is very little sunlight, the two cracks should behave similarly. As an initial test of this hypothesis, the solar radiation data from the LACMA weather station was examined. A day of low peak solar radiation theoretically corresponds with a cloudy, overcast day, and thus the effect of direct sunlight should be less noticeable.

During late spring and early summer a weather pattern known as "June Gloom" covers the coast of southern California with a thick marine cloud layer (UCSD, 2013). While this weather is more pronounced at the coast, and will often burn off by the early afternoon, on several days the marine layer will continue inland, reach Watts, and remain in the area for the duration of the day. For this reason, the search for overcast days started by looking at the data from the month of

June. Four days were selected: two days with low solar radiation and two days with high solar radiation. Through comparisons with the temperature data, these days also correspond fairly well with high and low temperature days.

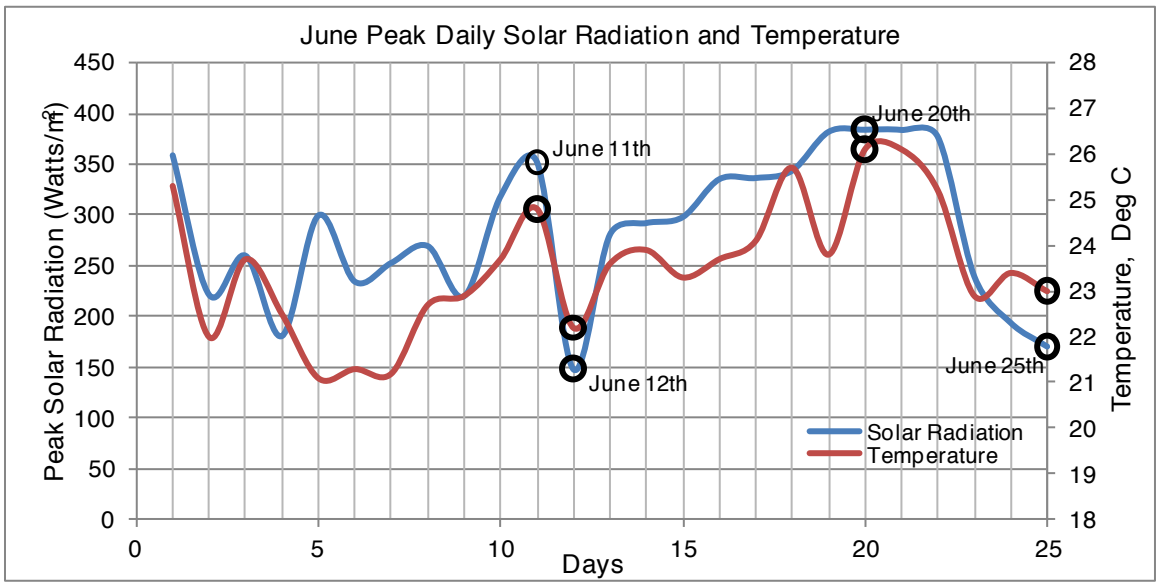

Figure 4.16: Peak daily solar radiation

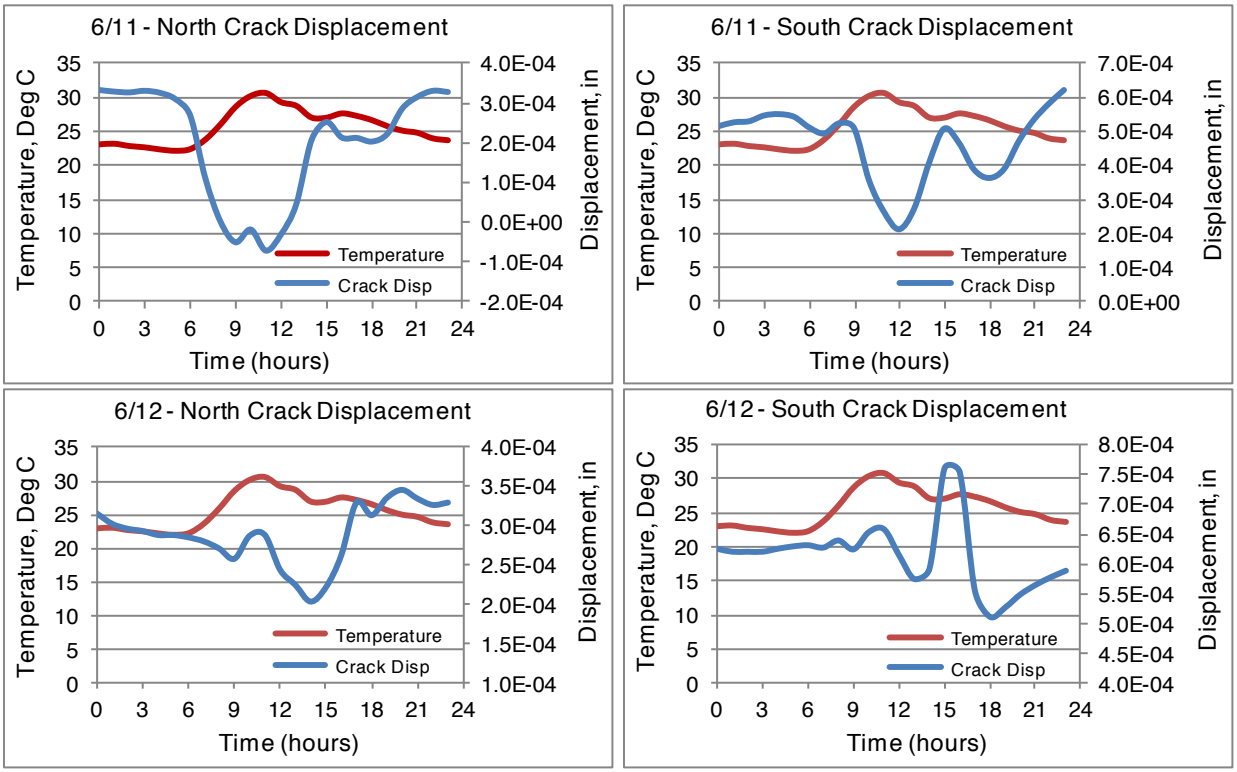

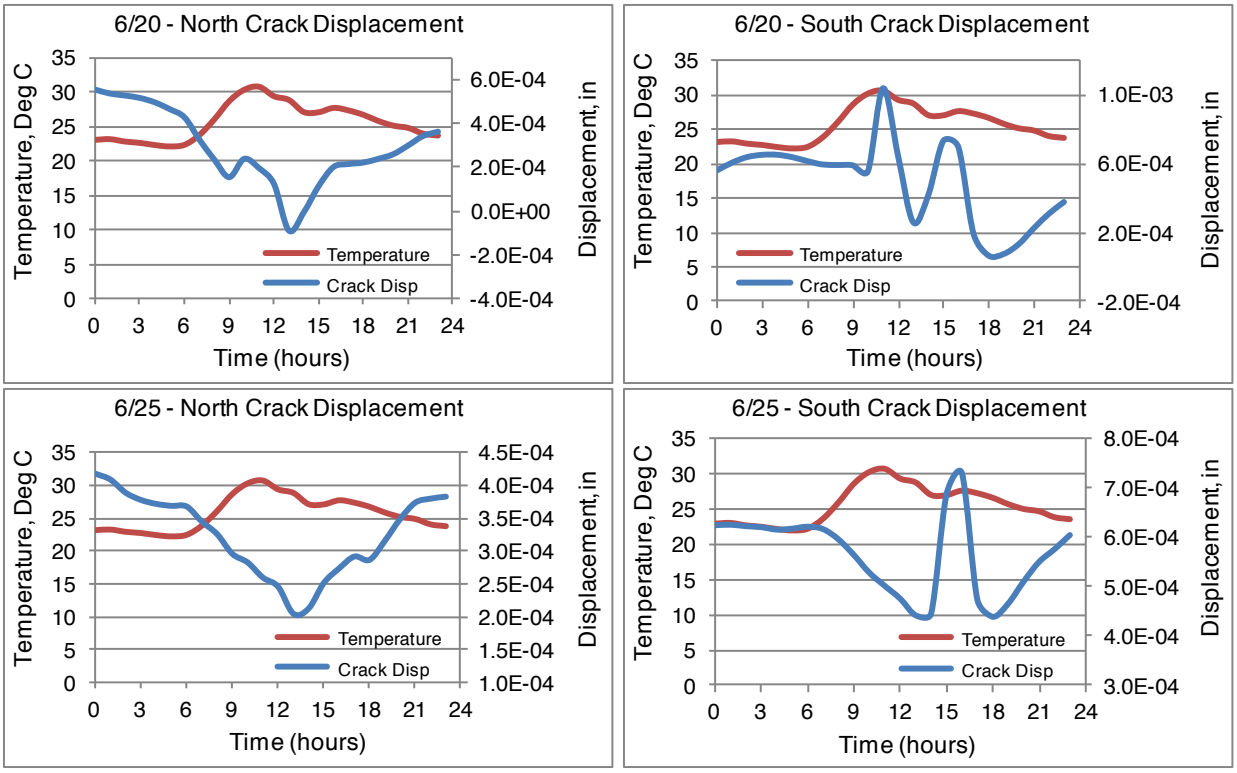

Figure 4.17: Selected daily crack displacement for high and low solar radiation days

Other than a few small deviations, the north crack follows the same pattern. On the two high radiation/temperature days, the north crack opened and closed a total of 0.0004 and 0.0006 inches. On the low radiation/temperature days, the displacements were much smaller—0.00014 and 0.0002 inches—suggesting a relationship between peak temperature and overall crack movement. The south crack follows roughly the same pattern on three of the four days, but on June 20 an abnormal opening is seen around 10 am. Other than that, they all follow the pattern of reaching a minimum around 12-2 pm, a maximum around 3-4 pm, and finally reaching a second minimum point around 6 pm. The total displacement on the hot days was 0.00041 inches and 0.00097 inches, whereas for the colder days, it was 0.00025 and 0.00029 inches.

These data show that the overall magnitude of the crack movement is dependent on the temperature or radiation, but a shift in behavior wasn't seen for the low radiation days. Even on low radiation/overcast days, the south crack will receive some direct sunlight, which may still

affect its behavior. In order to better test the effects of direct sunlight, a shade experiment was devised that involved covering the south-side crack with an 8'×12' double-layered canvas tarp as shown in the photographs below. The location of the crack sensor is circled in the right picture.

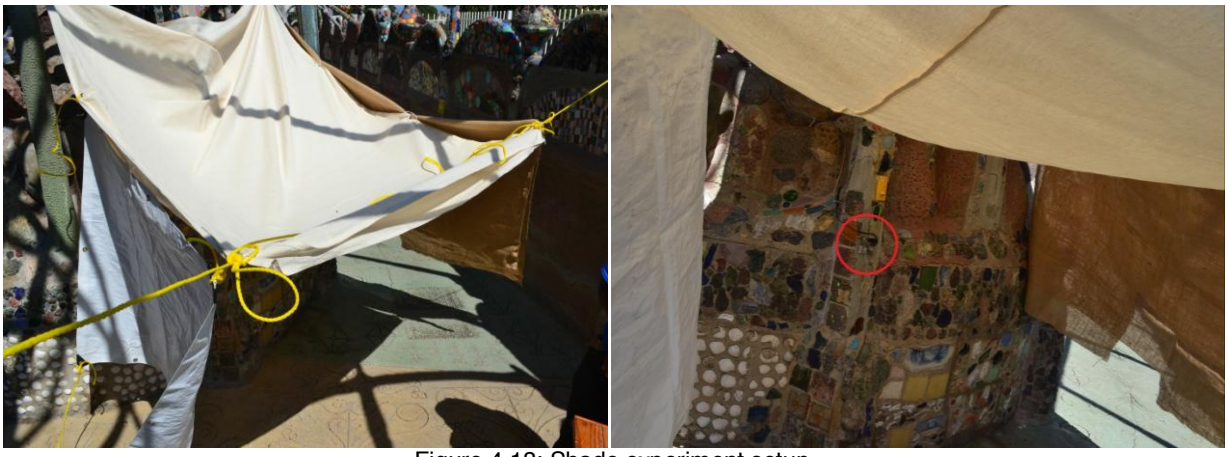

Figure 4.18: Shade experiment setup

The shade was setup in the afternoon of July 29 and left until the afternoon of July 31. Figure 4.19 shows the crack displacement from July 30, the day during which the crack was covered from beginning to end.

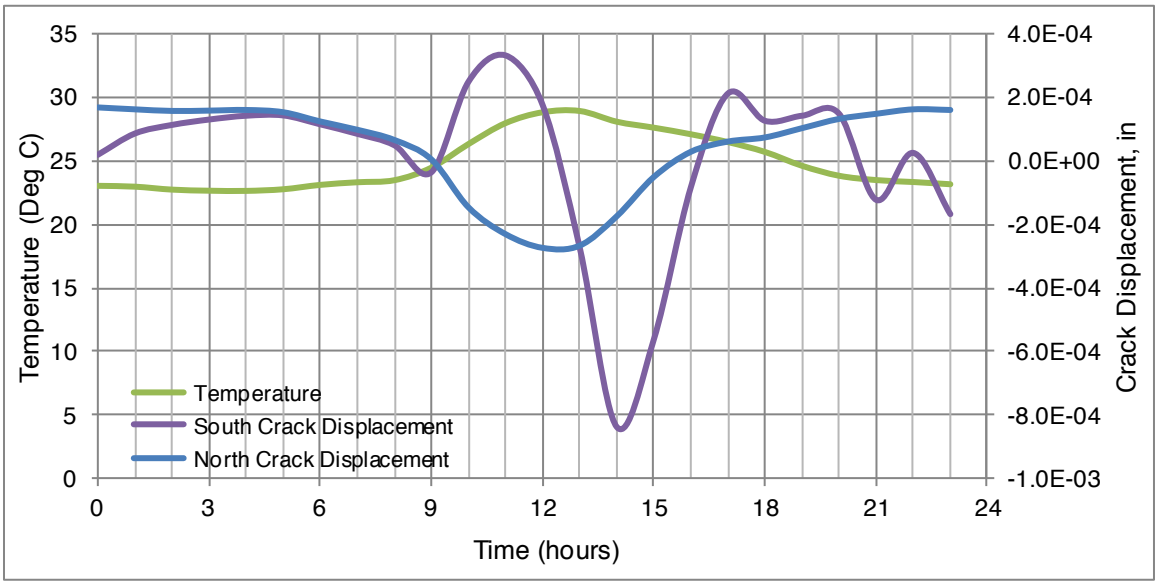

Figure 4.19: Shade experiment crack displacement results

If the hypothesis were entirely correct, the south crack's shape should be similar to that of the north crack. While this wasn't the case, the south crack still displayed a unique behavior that

wasn't observed on previous days. The initial opening around 10 am is similar to what was seen on June 20, but after reaching a minimum at 2 pm the crack reopens until 5 pm at which point it starts to oscillate around its equilibrium location. On a typical day, another closing cycle would have been observed. With only one full day of data to investigate, and a shape that is still highly irregular, it is not possible to conclude with certainty whether (or not) the direct sunlight exposure is the cause of the south crack's behavior. The shift in shape, nonetheless, lends credibility to the hypothesis. A better test of local heating effects could involve a larger, more reflective tarp that is attached higher up on the tower. It may also be possible to provide a small air-conditioning unit underneath the tarp, or other methods of controlling the local environment. The global tilting effects on crack movement can be further studied using the data from a rainy day. During a rainstorm, there will be extensive cloud cover, which will block the incoming sunlight and reduce the overall temperature during the middle of the day. The rain will also help to cool the structure, minimizing any differential heating between the two sides. If the south crack still behaved in a different manner than the north crack during these two cases, then it is possible that the unique behavior is a function of the column's construction. Differences in interior reinforcement and varying levels of deterioration may lead to differences in crack response.

One trend that was noticed in looking at the data is that the amount of movement on any given day depends on the overall peak temperature. On a hot day the crack will open and close to a greater extent than on a cold day. The peak daily crack movements, defined as the difference between the maximum and minimum displacements during the course of the day, were analyzed for the summer months (June – August). The results are shown in Figure 4.20.

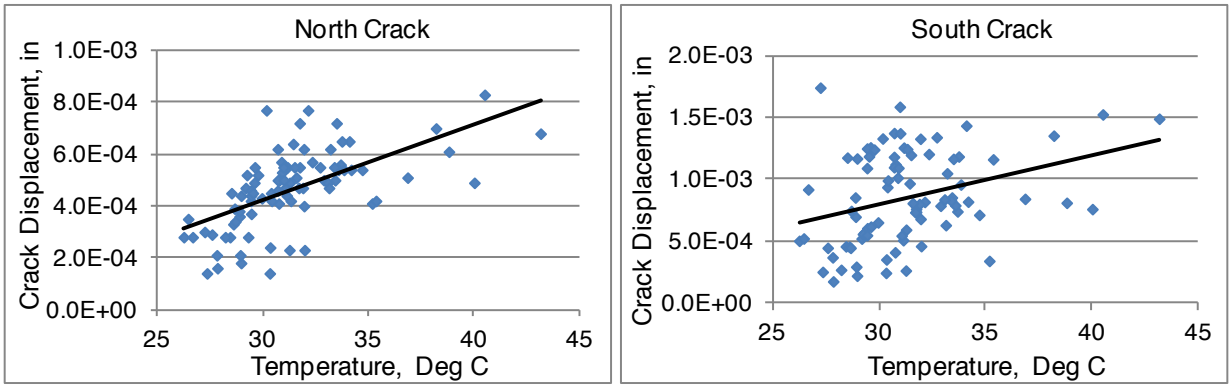

Figure 4.20: North and south crack peak daily displacements vs. temperature

For both cracks, there is a clear upward trend; higher temperatures lead to a greater amount of crack movement. Again, the north crack's behavior is more uniform whereas the south crack shows some scatter. The range of movement for the north crack is between 0.00014 and 0.00083 inches. The south crack's range is between 0.00017 and 0.0018 inches.

While it is difficult to ascertain whether or not thermal effects are the root cause of the cracks forming, a clear relationship between temperature and crack movement can be seen in the data. Over the course of the day, the cracks "breathe," undergoing daily closing and opening cycles with maximum magnitudes around 0.002 inches. In order to fix these cracks it is necessary to have a material that is flexible enough to move with the existing material and withstand these motions without allowing the crack to reopen.

5 Earthquake and Wind Response

The Watts Towers have stood the test of time against frequent small earthquakes, and a few large-amplitude earthquakes and windstorms. The vibrations during these events are occasionally high enough to knock off previously loosened ornaments (LACMA, 2012). Large enough vibrations and displacements may even be the initial cause of crack formation.

5.1 Earthquakes

The Watts Towers are located in southern California at 33.939°N latitude, 118.241°W longitude. This location is close to several major faults including the San Andreas, Newport-Inglewood, Raymond-Hollywood and Palos Verdes Faults. The following table summarizes a few major southern California earthquakes that have occurred since the Towers began to be constructed, and their distance to the Towers. Many of these earthquakes caused visible damage to the Towers (Goldstone, 1997).

Table 5.1. Notable Earthquakes in Proximity of the Towers

Name	Year	Mag.	Epicenter Latitude	Epicenter Long.	Distance (km)
Long Beach	1933	6.4	33.63	-117.99	25.8
Kern	1952	7.5	35.00	-119.01	137.5
Sylmar	1971	6.6	34.24	-118.24	20.8
Whittier Narrows	1987	5.9	34.06	-118.08	20.1
Sierra Madre	1991	5.8	34.26	-118.00	42.1
Landers	1992	7.3	34.13	-116.26	114.3
Big Bear	1992	6.5	34.20	-116.82	84.5
Northridge	1994	6.7	34.12	-118.32	13.3
Hector Mine	1999	7.1	34.59	-116.27	121.3
Inglewood	2009	4.7	33.94	-118.35	6.3
Pico Rivera	2010	4.4	33.99	-118.08	9.8

Note that the 1933 Long Beach Earthquake ruptured the Newport-Inglewood Fault, with surface rupture observed within 2 miles of the Watts Towers. The towers were in the early stage

of construction then, and the damage is not well-documented. Shaking would have been very strong during that earthquake, as it would be for future earthquakes on the Newport-Inglewood Fault. By studying historical photographs and the interior structure of the Towers, Goldstone (1997) concludes that Rodia made significant changes to his design following the Long Beach earthquake. He added six new columns and more than fifty new bands on the East and Center Towers. Many of the overhead arches that connect the Center and East Towers and all the towers to the surrounding walls were added during this time as additional stability.

Due to the high seismicity in this area, it was hoped that several earthquakes would occur during the duration of the UCLA monitoring. Unfortunately, as of now, only a few small earthquakes have been recorded. The most notable was the March 11, Anza Earthquake, which was a M4.7 earthquake with an epicenter approximately 172 km from the Towers. The acceleration and tilt responses to this earthquake are shown in Figures 5.1 and 5.2.

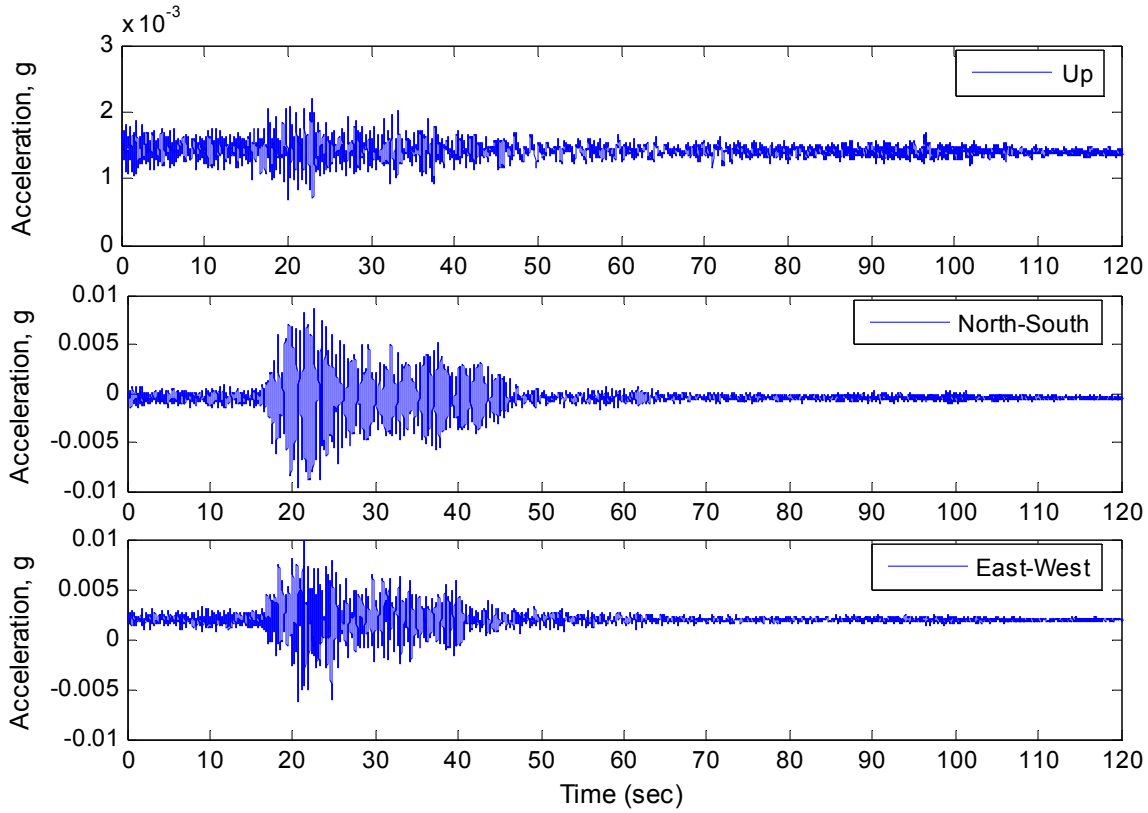

Figure 5.1: Acceleration response to the March 11, 2013, Anza Earthquake

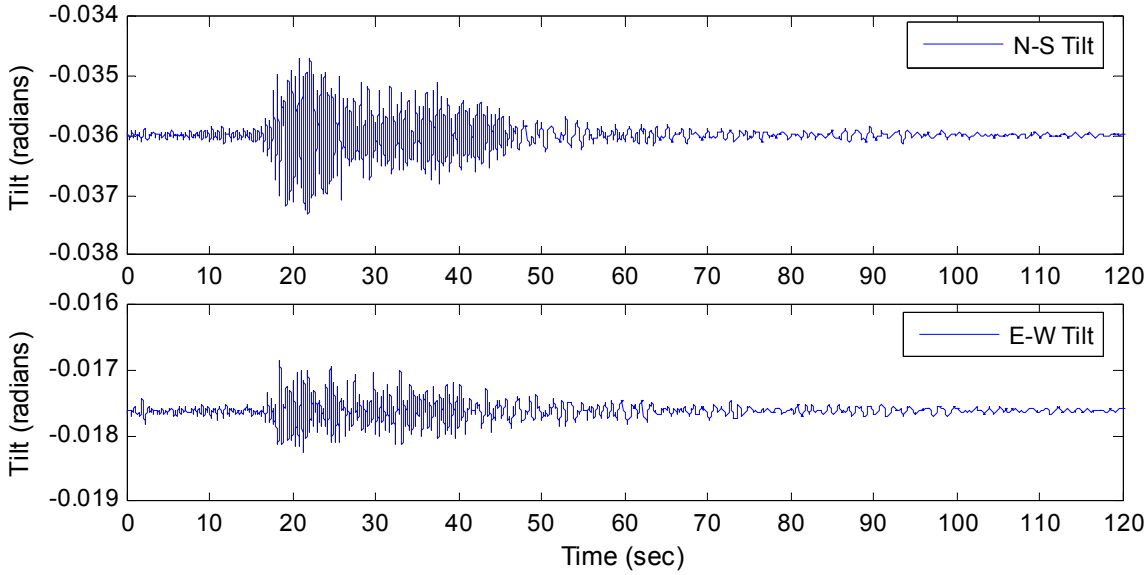

Figure 5.2: Tilt response to the March 11, 2013, Anza Earthquake

Both the N-S and E-W components of acceleration reach approximately 0.01g, while the vertical component is much smaller and only reaches a maximum of 0.001g. This vibration is reasonably low, but is approximately 10 times larger than the ambient vibrations. The earthquake clearly registered on the tilt sensor as well, with peak-to-peak movement of about 0.002 radian in the N-S direction. Using the previously derived cantilever approximation (Eq 4.5), these tilt values result in around 3.1 inches of displacement at the tip of the Central Tower.

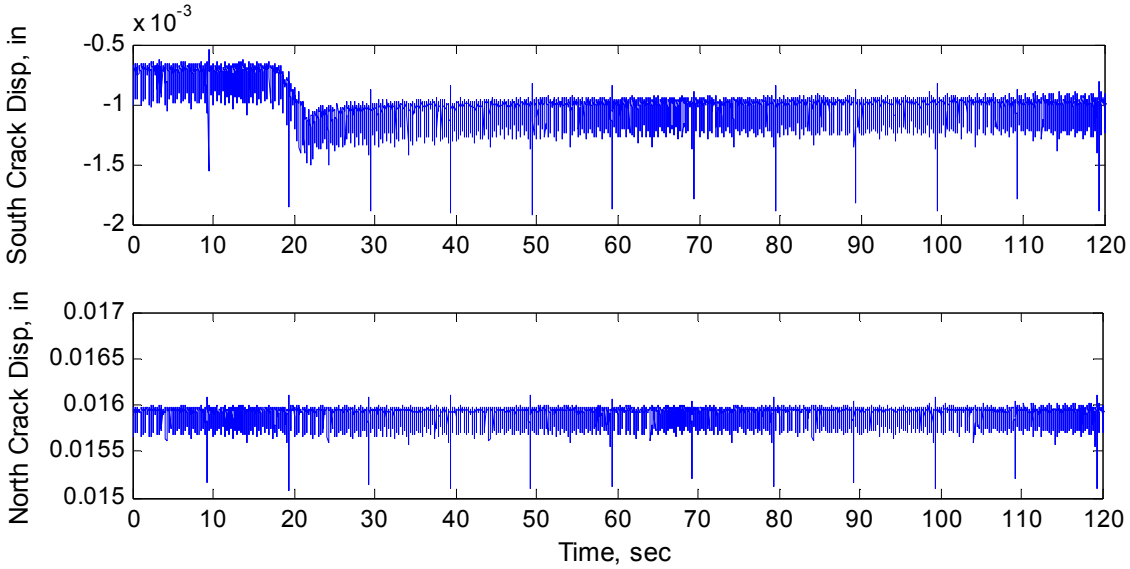

Figure 5.3: Crack displacement response to the March 11, 2013, Anza Earthquake

Figure 5.3 displays the south and north crack displacements during the earthquake. In the south crack, there is a noticeable closing movement around 18 seconds, which corresponds almost exactly with the first pulse of the earthquake. Unfortunately, this small-amplitude data is from the period in which the displacement sensors had a noisy power supply that reduces the precision of the measurements.

It has been seismically very quiet in Los Angeles so far in 2013. One target of the continued data collection at Watts Towers is to capture larger-amplitude earthquake shaking with improved precision.

5.2 Wind

Other than a few trees on the west side of the site and scattered throughout the neighborhood, the Watts Towers are surrounded in every direction by low-rise (one- and two-story) residential construction. This means that there are no significant objects that can break the winds, and thus, the 100-foot tall towers nominally face the full force of the northerly Santa Ana winds. In April 2013, a windstorm hit the towers with speeds peaking over 30 mph at the height of the wind sensor, which is approximately 15 feet. The following plots show the wind speed, acceleration, tilt, and crack response during a four-minute period of high wind gusts.

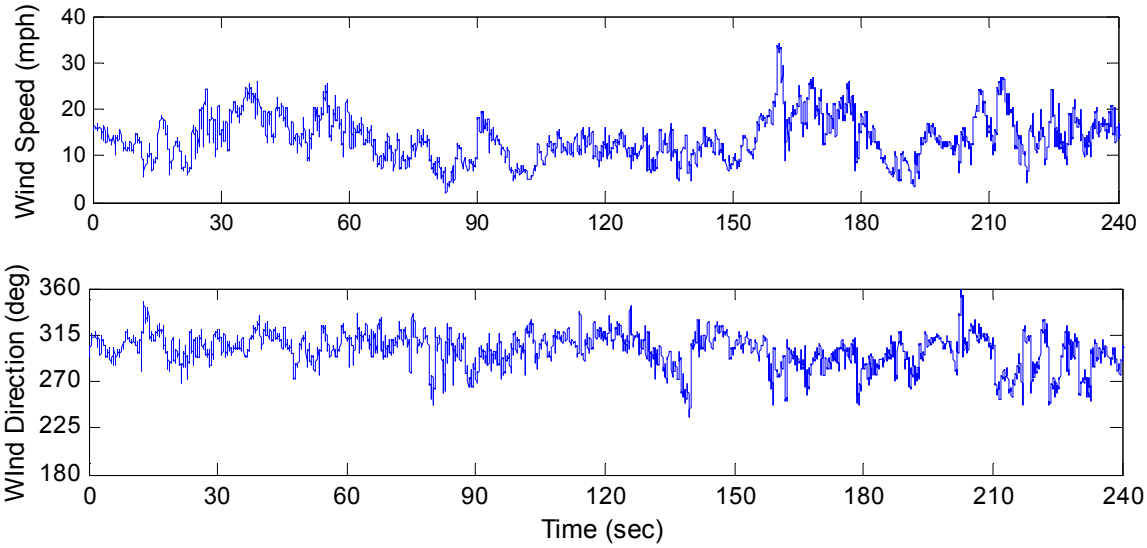

Figure 5.4: Wind speed and direction

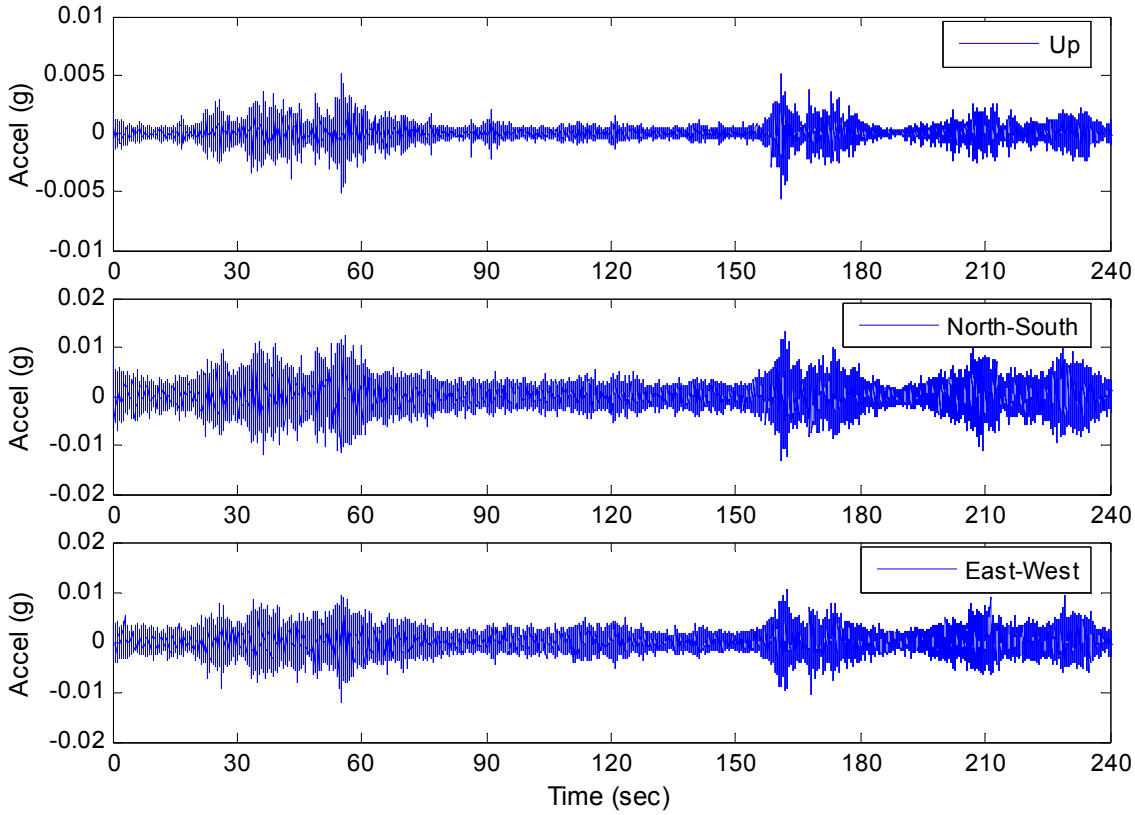

Figure 5.5: Wind storm acceleration response

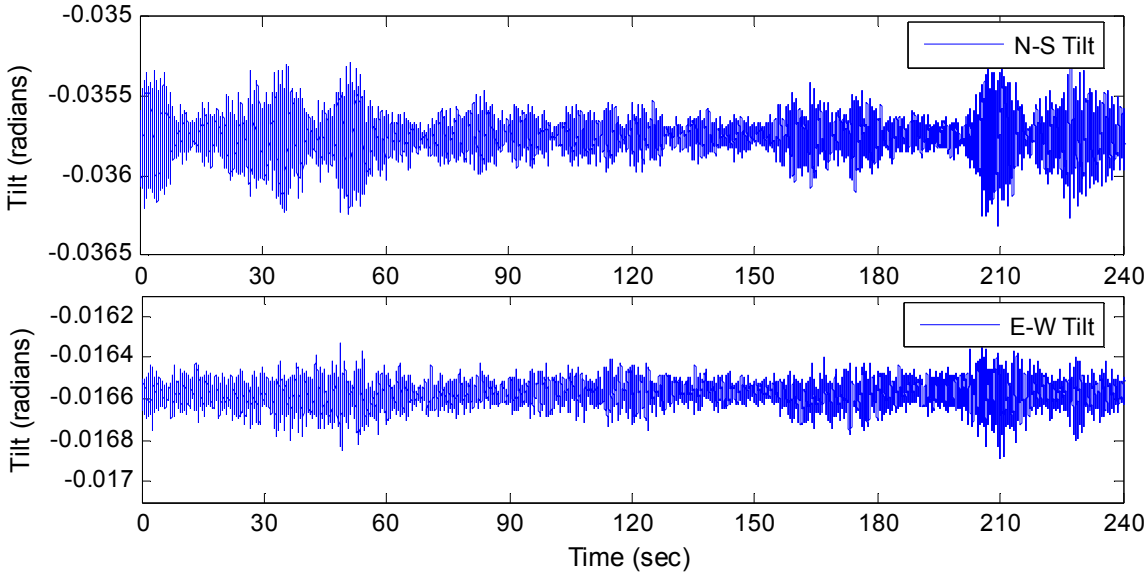

Figure 5.6: Wind storm tilt response

The primary wind direction is northwest, with the strongest acceleration response in the north-south direction. The peak accelerations in the N-S and E-W directions are 0.016*g* and 0.014*g*, respectively. The peak-to-peak tilt magnitudes are 1×10^{-3} radians and 5×10^{-4} radians in the N-S and E-W directions, respectively, which yield approximate tip displacements of 1.56 inches and 0.78 inches. When compared to the earthquake response, the windstorm resulted in larger accelerations, but the magnitude of tilt was smaller. Looking at the plots for crack displacement in Figure 5.7, other than a small shift in the south crack, this wind storm doesn't appear to have dynamic affect on the crack movement.

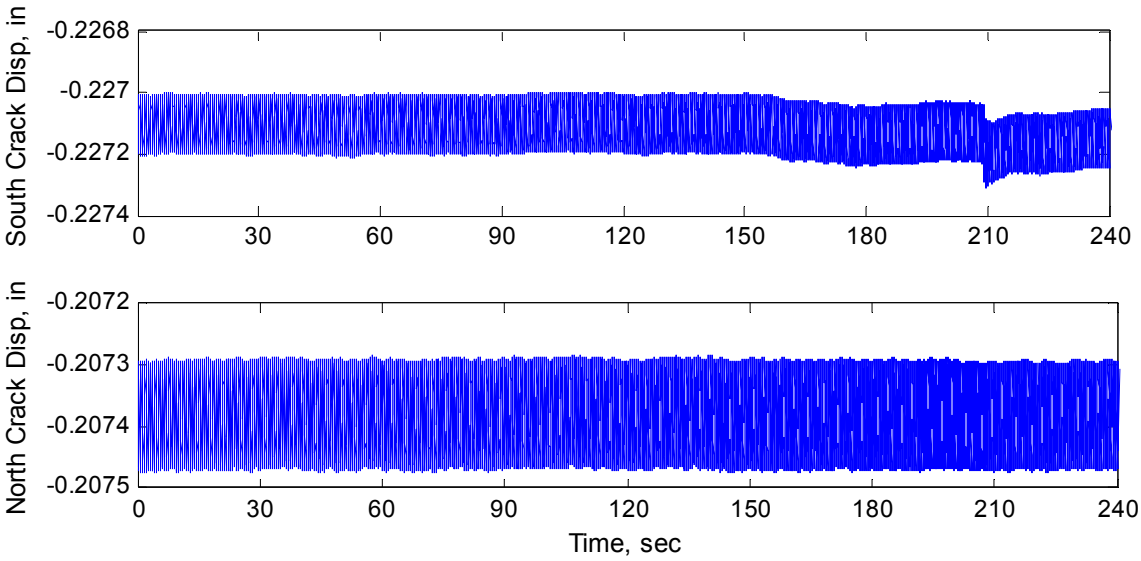

Figure 5.7: Wind storm crack displacement response

Data collection will continue through the fall and into winter, the two seasons when Santa Ana winds are likely to peak. With additional data during future wind events, a more definite conclusion can be made on whether the instrumented cracks are affected by high winds.

6 Behavior of East and West Towers

On July 30, the three towers were instrumented with a total of five triaxial accelerometers—four new ones plus the one that was previously installed—as shown in the figure below. Two goals of this sensor arrangement were to quantify the amount of coupling between the towers, as well as to estimate the stiffness of the East and West Towers by finding their fundamental frequencies.

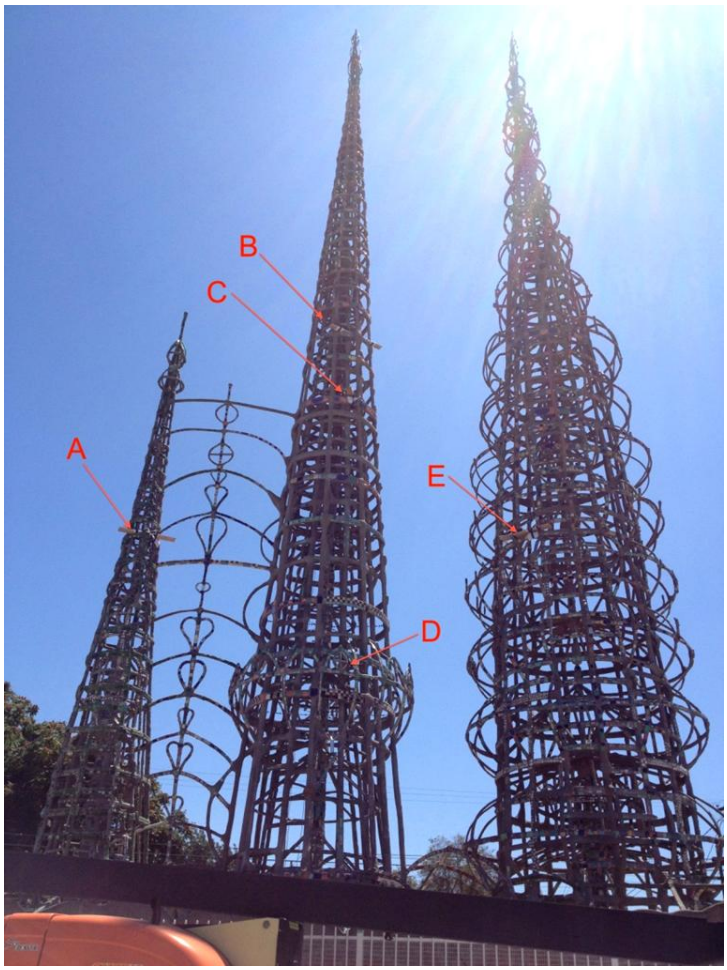

Figure 6.1: Sensor arrangement (all three towers)

Table 6.1. Sensor Locations

Label	Tower	Height (feet)
A	East	32.7
B	Center	52.2
C	Center	45.1
D	Center	22.8
E	West	33.6

A total of 12 beams span the gap between the East and Center Towers, starting at a height of 11 feet and ending near the top of the East Tower at just under 45 feet. It was hypothesized that these beams would lead to a strong coupling of motion between the two towers, with the

taller, heavier Center Tower driving the motion of the smaller East Tower. There are also a few smaller overhead arches that connect the Center and West Towers around the 8-10 foot elevation. Since these arches are near the base of the towers, where the structures are very stiff, it is unlikely that they will lead to significantly coupled motions. In order to test the amount of coupling, one of the exterior columns along the base of the Center Tower was shaken by hand, first in the N-S direction and then in the E-W direction.

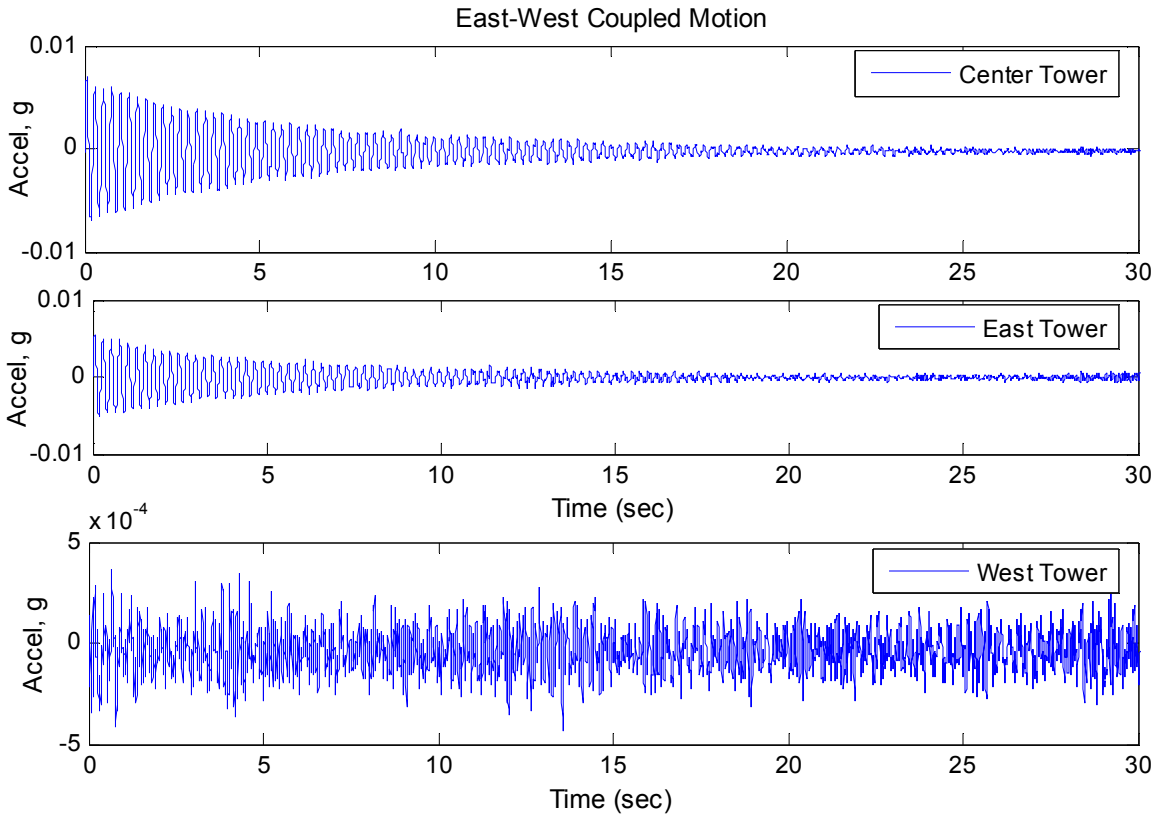

Figure 6.2: East-West acceleration transfer between towers

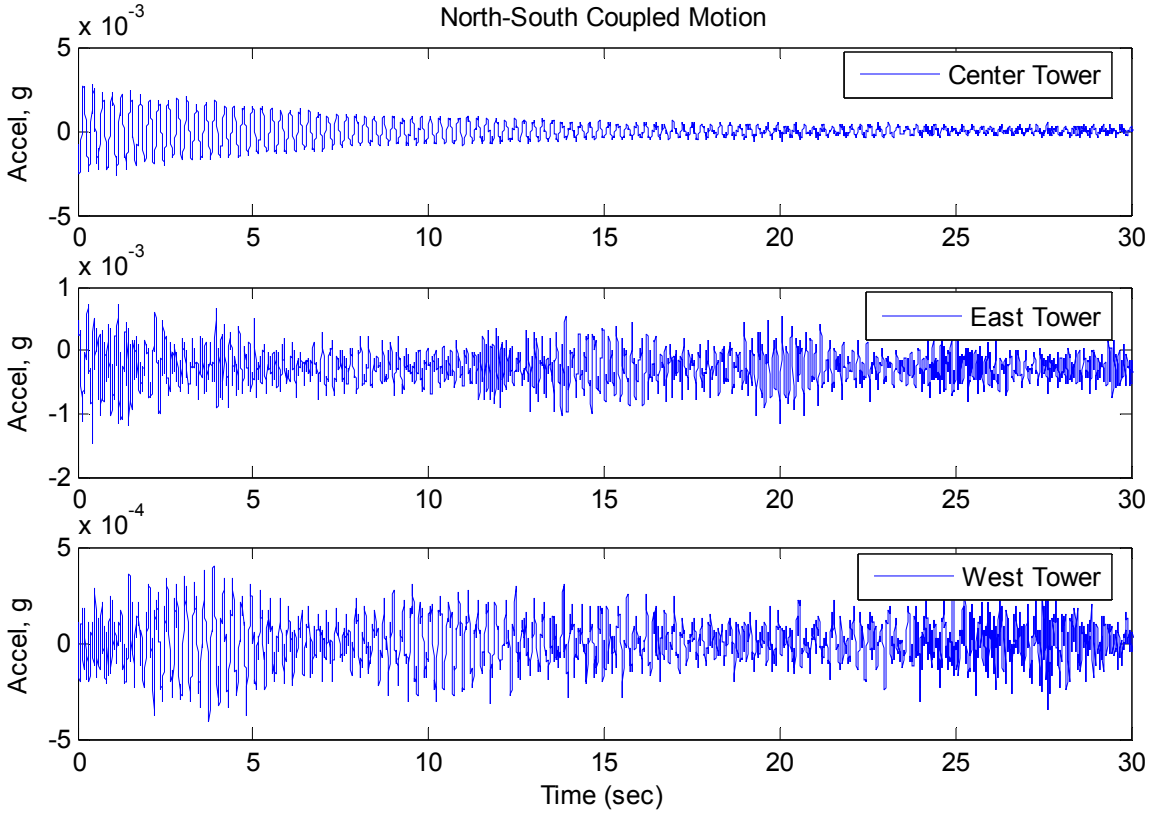

Figure 6.3: North-South acceleration transfer between towers

In the east-west direction the coupling is immediately clear between the East and Center Towers. The peak acceleration from sensor D on the Center Tower was 0.011*g*. The peak acceleration on the East Tower was 0.0086*g*, nearly 80% of the acceleration on the Center Tower. This proves the hypothesis of the two towers (Center and East) being significantly coupled. When looking at the response of the West Tower, only a small increase above the ambient vibration is seen; the peak acceleration is only 6% of that on the Center Tower. This suggests a negligible coupling between the West Tower and the Center Tower. In the north-south direction the coupling is also negligible. Any coupling in this direction would be dependent on the flexural stiffness of the connecting beams. Since these elements are long and fairly slender, their flexural stiffnesses are very low.

The `pwelch` function was again used in Matlab in order to obtain the averaged power spectral density of the East and West Tower acceleration signals and to estimate the fundamental frequencies. The resulting plots are shown below. Note that in order to visualize the coupling of the Center and East Towers in the frequency domain, the Center Tower's PSD is plotted along with the East Tower's.

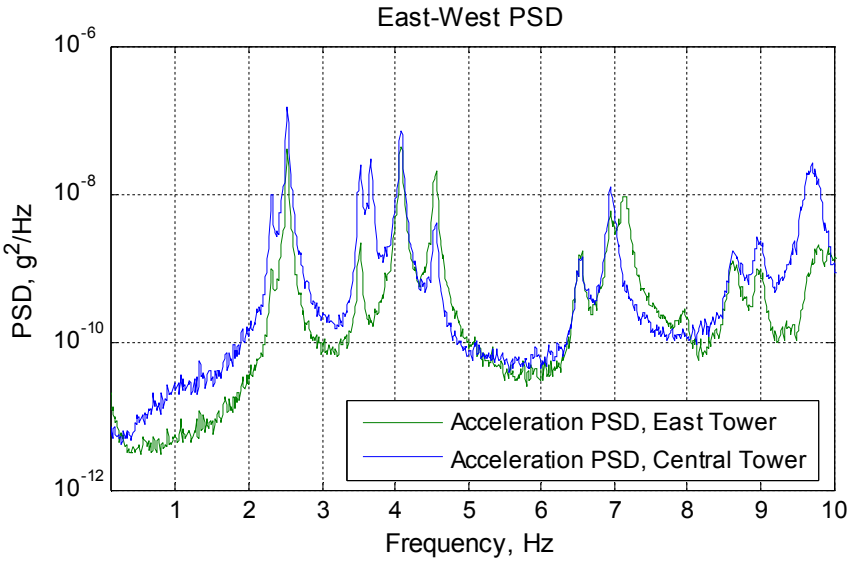

Figure 6.4: Central and East Tower power spectral density, east-west

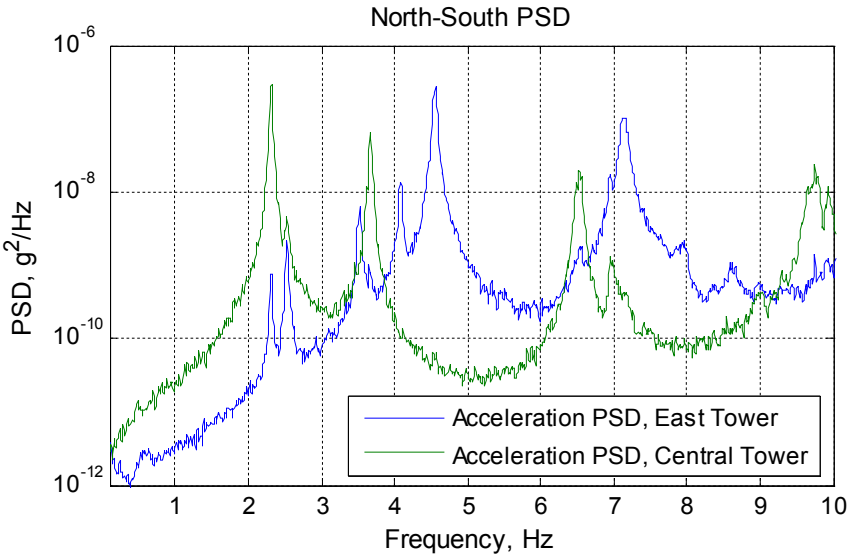

Figure 6.5: Central and East Tower power spectral density, north-south

The coupling is again very clearly shown by plotting the east-west PSD's of the two towers together in Figure 6.4. At each mode for one of the towers, there is a corresponding peak in the PSD for the other tower, although the magnitudes of the peaks vary between the two. The PSD in the north-south direction (cf. Figure 6.5) clearly shows the difference in the East and Central Towers. The East Tower is approximately 40 feet shorter than the Central Tower, and is therefore much less flexible. The first two frequencies for the East Tower are at 4.56 Hz and 7.13 Hz.

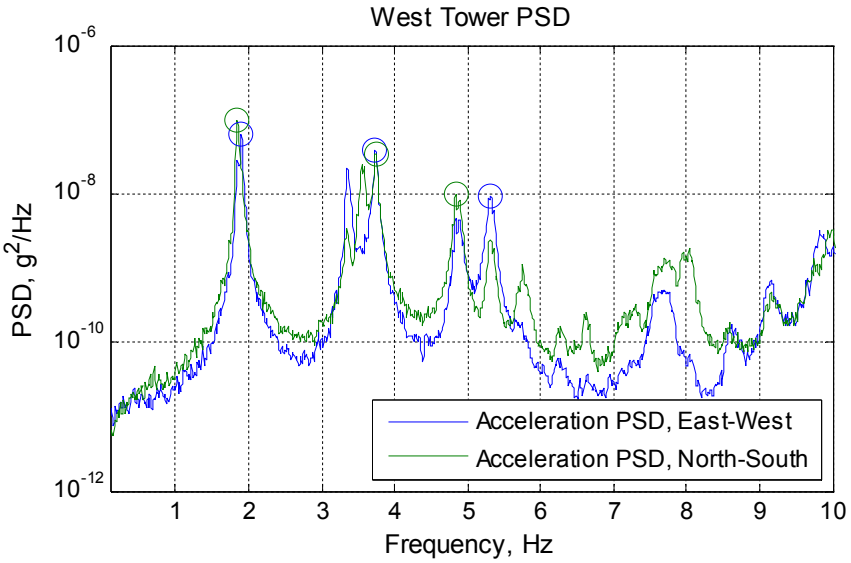

Figure 6.6: West Tower power spectral density

The West Tower has the lowest frequencies. The West and Central Towers are similar in height and weight, but the West Tower has a more open construction with only 16 columns arranged in one layer, and fewer bands and spokes, resulting in a reduced stiffness. The West Tower was the last one built (Goldstone, 1997), and it is possible that the experience gained from building the first two towers helped to give Rodia the confidence to build a more open, less redundant structure. Note that since the West Tower is uncoupled from the other two, its spectrum is almost perfectly symmetrical between the E-W and N-S directions.

A further benefit of the manual excitation test of the Center Tower has been regarding the estimation of structural damping. The acceleration measurements in Figures 6.2 and 6.3 display a clean exponentially decaying signal. Approximating the Center Tower as a single degree-of-freedom (SDOF) oscillator allows for a closed form solution to this motion. Elastic vibration theory states that an SDOF structure will undergo free vibration decay according to the following formula (Chopra, 2007):

$$u(t) = e^{-\xi\omega t}\left[u_o \cos(\omega_d t) + \frac{\dot{u}_o + \xi\omega u_o}{\omega_d}\sin(\omega_d t)\right] \tag{6.1}$$

where ω and ω_d are the undamped and damped frequencies, u_0 and $\dot{u}_o$ denote the initial displacement and initial velocity, and ξ is the damping ratio, expressed as a percentage of critical damping. When the damping ratio isn't known, the above equation can be used to derive the so-called log-decrement approach which estimates the damping according to the following equation:

$$\xi = \frac{1}{2\pi}\ln\frac{u_n}{u_{n+1}} \tag{6.2}$$

where u_n is the peak displacement for one cycle, and u_{n+1} is the displacement at the next peak. A segment of the acceleration signal from Sensor D was filtered and double integrated using a trapezoidal sum in order to find the displacement. The resulting displacement values were used to estimate the damping ratio of the Center Tower.

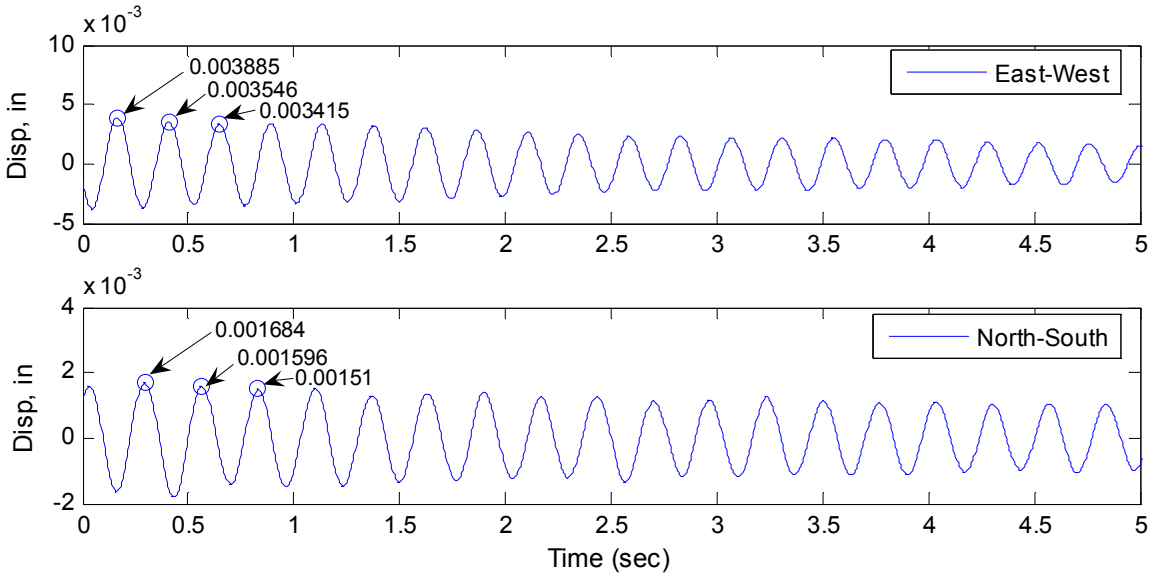

Figure 6.7: Log decrement damping approximation

East-West:

$$\xi = \frac{1}{2\pi}\ln\frac{0.003885}{0.003546} = 1.5\%$$

$$\xi = \frac{1}{2\pi}\ln\frac{0.003546}{0.003415} = 0.6\%$$

North-South

$$\xi = \frac{1}{2\pi}\ln\frac{0.001684}{0.001596} = 0.9\%$$

$$\xi = \frac{1}{2\pi}\ln\frac{0.001596}{0.001510} = 0.9\%$$

Per this approximate method, the damping appears to be in the 0.5-2% range. Typical values for reinforced concrete vary between 2% and 5% depending on the amount of reinforcement and cracking (Newmark and Hall, 1982). The estimated damping is on the low side, but is still within a reasonable range for this hybrid structure.

7 Computer Modeling

The results of the environmental and vibration monitoring of the Central Tower have provided a wealth of data on how temperature affects the tower's frequencies, tilt, and crack displacements. The data can only tell part of the story, however, since the measurements are specific to a certain location and extrapolating the results, such as to find the tip displacement of the tower given the tilt, involves making several assumptions. A calibrated finite element model can be used to study additional trends such as stress distributions, as well as global and local displacement patterns during thermal loading. The initial model will assume linear elastic behavior, an adequate assumption for the low-level environmental effects that will be studied. If deemed necessary, the model could later be updated to include nonlinear effects, which would require accurately inputting the assumed material behavior (initial strength, post-yield strength, hysteretic behavior, damping, etc). While the initial model will only include the Central Tower, the same procedure used to develop the model could be used to model the other two towers as well.

In order to create the computer model, it was first necessary to define the geometry. A laser scan of the Watts Towers site, completed in October 2011 by GBG USA (GBG USA, 2011), aided in this process. The results of this scan were used to estimate the cross-sectional areas, lengths, and connectivities of the elements that make up the structure.

7.1 Laser Scan

A laser scan works by having a transmitter send out a laser beam, or other light source, and then recording the time it takes for the signal to return. Using this information, it is able to estimate the distance from the transmitter to a certain point in space. Rotating the head of the transmitter by very small angles in the horizontal plane, while a rotating mirror redirects the beam in the

vertical plane, allows a laser scanner to quickly measure the distance to many points in 3D space with very high accuracy (National Oceanic and Atmospheric Administration, 2012). Moving the transmitter to several different locations around a site allows the geometry to be captured from every angle.

The resulting output from a scan is commonly referred to as a "point cloud," which is simply a collection of points that include a 3D location in space, as well as an intensity value that allows the visualization of colors in the scanned image. The data points are typically very close to each other, resulting in an extremely large amount of data, even for a relatively small site. The Watts Towers scan, for example, has yielded over 295 million data points. The following figure displays the completed scan.

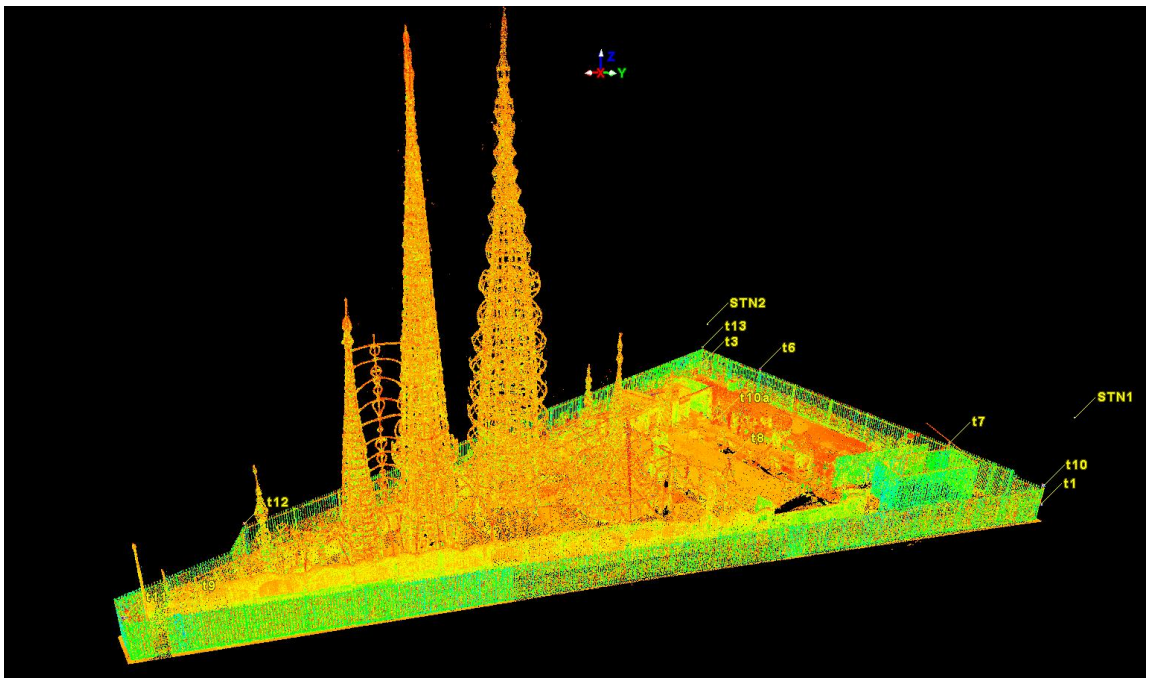

Figure 7.1: Laser scan of the Watts Towers site

The results of this scan were compared with a 2005 scan and two visual surveys completed in 1988 and 1994. The tops of the three towers showed displacements between 0.15” and 0.18”, well below the associated error of these measurements (LACMA Q5 Report, 2012), and also

well below the thermally induced daily movement. This suggests that there has been no long-term, permanent deformation of the towers.

7.2 Defining Model Geometry

When examined closely, the Towers are made of a few typical types of members that are repeated at semi-regular intervals. For the case of developing the model, the same naming convention for these members was used that was previously used in the Ehrenkrantz Preservation Plan (Ehrenkrantz, 1983). The members are as follows:

- **Center Core**: large column at the center of the tower that runs vertically over the entire height
- **Columns:** vertical members surrounding the center core that are typically arranged in three layers (interior, intermediate and exterior).
- **Bands**: horizontal members surrounding the columns that help to provide bracing to the columns
- **Sub-Band**: a band that only goes around part of the tower's circumference.
- **Spokes**: any member that connects a column (typically the center core) to a band or column. These act along with the braces to provide additional stability.
- **Braces**: any member connecting two intermediate or exterior columns
- **Loops**: any member, typically connected to an exterior column or band, that arches away from the structure.

Figure 7.2: Tower member labels

The first step for defining the geometry was to isolate the Central Tower from the rest of the laser scan. It was then further subdivided into 10 sections over its height that could be processed

one at a time. Distances and locations were found by selecting a point, or a number of points, in the point cloud and manually recording the (x,y,z) coordinates. A number of simplifications were made in order to ease the geometry definition and model development. The typical steps and simplifications are as provided in what follows.

Steps for defining column member locations and areas:

1. A horizontal cut is made at the beginning of each one of the 10 sections.

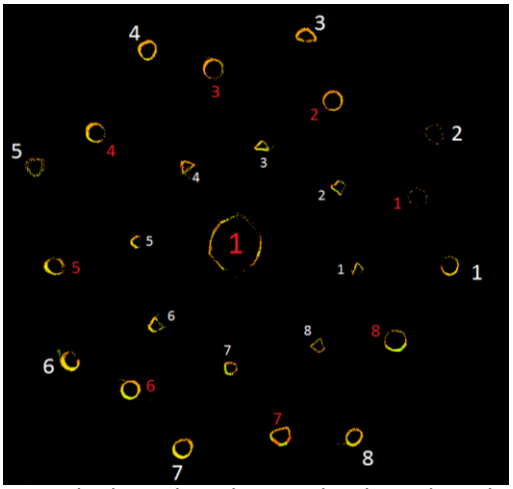

Figure 7.3: Laser scan horizontal section cut showing column locations

2. The (x, y) coordinates of the center are found for each member with the location of the center column being normalized to (0, 0).
3. The radial distance and angle of each column from the center column is calculated.
4. The average radial distance to a set of exterior, intermediate, or interior columns is found and a new location for each column is calculated using the average radius and the previously defined angle.
5. The location of the columns at any location between two sections is found by linear interpolation.
6. All columns were assumed to have a circular cross-section.
7. The diameter of each column was found at the location of the cut. The average diameter of a given set (exterior, intermediate, or interior) was found and uniformly applied to that set within each section.

The following table shows the organized data for the exterior columns in section 3. The starting location and diameter were manually entered. The distance from the center column and the new approximate location were then calculated in a spreadsheet. The default units in the laser scan were meters, which are the units presented in the following table.

Table 7.1. Section 3 - Exterior columns locations

Center Column	Starting Point (m) x	y	Diameter (m)						
	545.053	513.812	0.331						
Exterior Columns	Starting Point (m) *x*	*y*	Diameter (m)	Distance from center post (m) *x*	*y*	*r*	*Θ (deg)*	Approximate Location (m) *x*	*y*
1	546.518	513.646	0.102	1.465	-0.166	1.474	353.53	1.459	-0.165
2	546.350	514.563	0.111	1.297	0.841	1.546	32.96	1.232	0.799
3	545.517	515.214	0.099	0.464	1.402	1.477	71.69	0.461	1.394
4	544.419	515.122	0.109	-0.634	1.310	1.455	115.83	-0.640	1.322
5	543.669	514.295	0.107	-1.384	0.483	1.466	160.76	-1.386	0.484
6	543.906	513.050	0.109	-0.147	-0.762	1.377	213.60	-1.223	-0.812
7	544.731	512.414	0.115	-0.322	1.398	1.435	257.03	-0.330	-1.431
8	545.843	512.519	0.095	0.790	-1.293	1.515	301.42	0.765	-1.253

For example, looking at Exterior Column 1:

Starting Point: (x , y) = (546.518 , 513.646) Center Column: (x , y) = (545.053 , 513.812)

Distance from Center Post (meters):

$$x = 546.518 - 545.053 = 1.465$$
$$y = 513.646 - 513.812 = -0.166$$
$$r = \sqrt{x^2 + y^2} = \sqrt{1.465^2 + 0.166^2} = 1.474$$
$$\theta = \tan^{-1}\left(\frac{x}{y}\right) = \tan^{-1}\left(\frac{-0.166}{1.465}\right) = -6.47° = 353.53°$$

Approximate Location:

$$r_{avg} = 1.468$$
$$x_{approx} = r_{avg}\cos(\theta) = 1.468\cos(353.535°) = 1.459$$
$$y_{approx} = r_{avg}\sin(\theta) = 1.468\sin(353.535°) = -0.165$$

Calculate Error in approximate location:

$$Error(x) = \frac{1.459 - 1.465}{1.465} = -0.41\%$$

$$Error(y) = \frac{-0.165 + 0.166}{-0.166} = -0.60\%$$

Steps for defining the horizontal band location:

1. The horizontal bands were classified based on the set of columns which they wrapped around (exterior, intermediate, interior).
2. A vertical slice was made to see the cross-section of each member.
3. The height of the centroid for each band was found and then the circumference was found based on the previously defined column radial arrangement.
4. All horizontal bands were assumed to have a rectangular cross section.

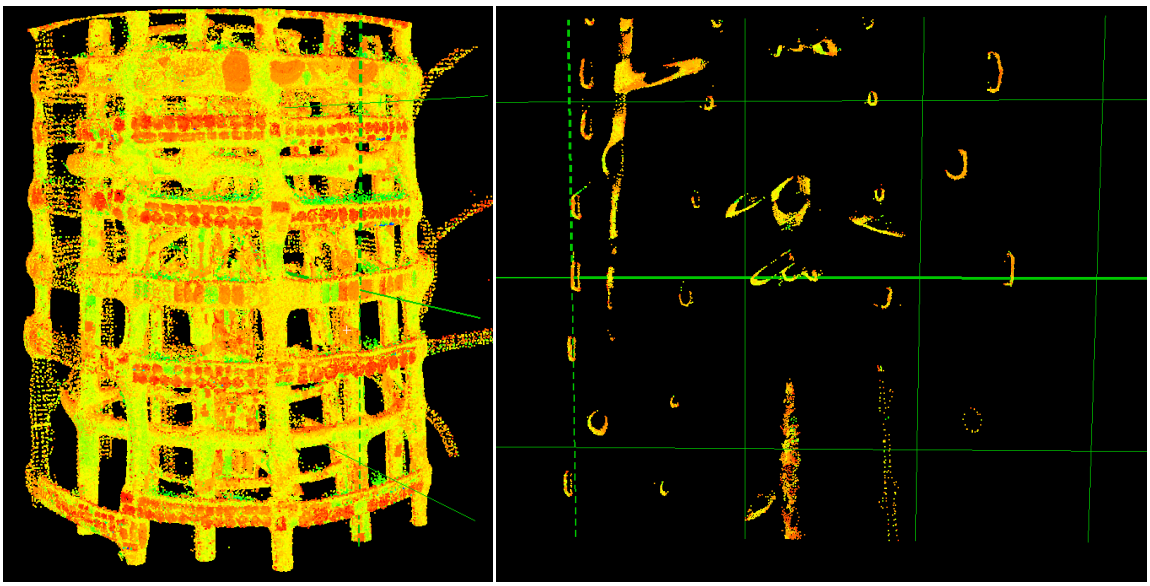

Figure 7.4: Vertical section cut showing band cross-sections

Steps for defining the spokes' locations and cross-sections:

1. The starting and ending location was found for each spoke
2. Spokes were assumed to be linear between the connection to the columns and the connection to the center core.
3. All spokes were assumed to have a circular cross-section.
4. The average diameter was found for each set of spokes (typically 8 members) and assigned to each member within that set.

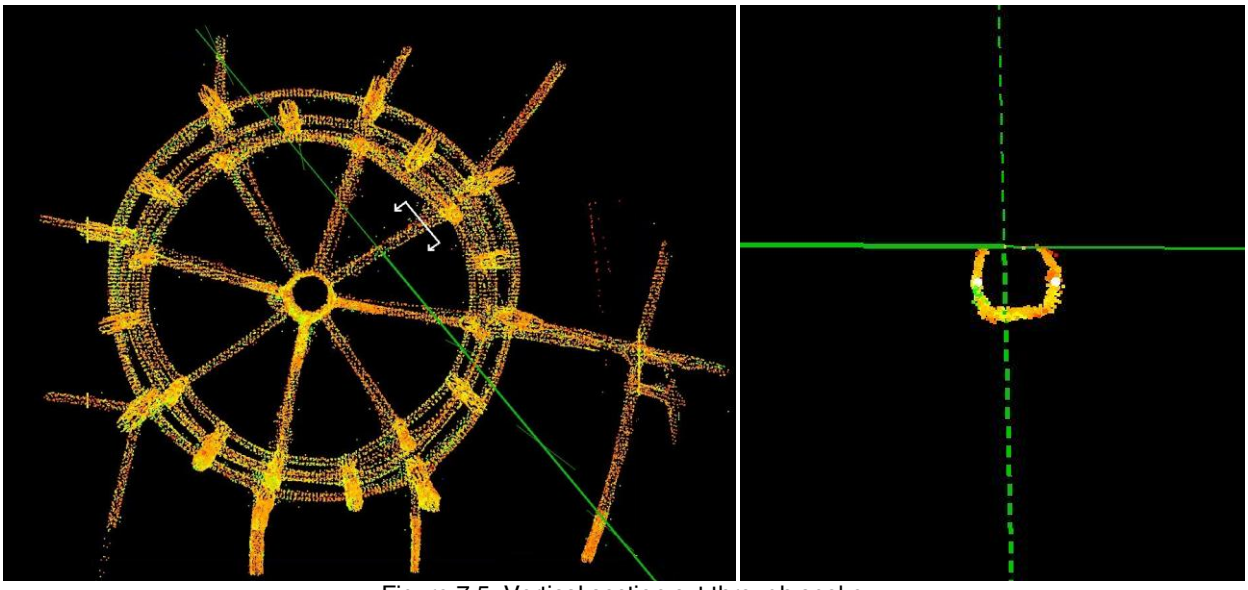

Figure 7.5: Vertical section cut through spoke

The bottom of each column is embedded into the heavy base of the tower; therefore, a fixed base boundary condition was assumed. The location of fixity was selected approximately 3 feet from the ground as shown in Figure 7.6.

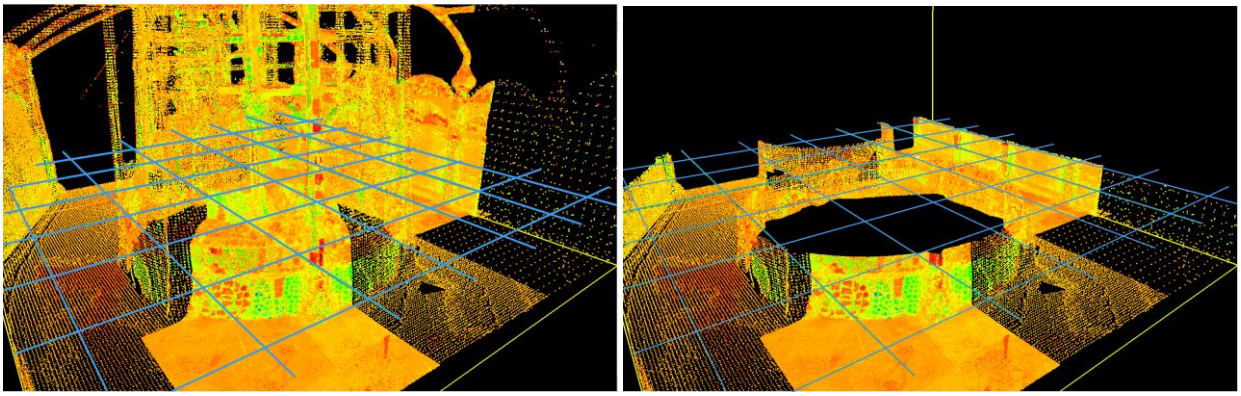

Figure 7.6: Assumed point of fixity for base boundary condition

Using these procedures, each member was named, assigned cross-section properties, and given a set of nodal coordinates. This information was then input directly into Abaqus, which is a proprietary finite element modeling analysis software package (Dassault Systemes, 2013), to define the model geometry.

7.3 Estimation of Structural Properties

The assumed material properties within a model can greatly impact the results. Even a model of a simple building that was constructed using modern materials will have a degree of uncertainty over the as-built material properties and overall behavior. The uncertainty is much higher for a structure as complicated as the Center Tower, built with a wide variety of materials over an extended period, and subjected to deterioration and several rounds of repair over the past 60 years. The model here will first be developed using the information on reinforcement and the concrete cover that is available, and will then be updated such that the modeled behavior matches the observed behavior within a reasonable error.

The Towers were constructed using an assortment of steel sections that were wrapped with a steel-wire mesh and then covered with a cement mortar. Two of the main structural elements used in the exterior columns of the West Tower were a 2-1/2×2-1/2×5/16 Steel Tee member and a 2×2×1/4 Steel Angle (Goldstone, 1963), with cross-sectional areas of 1.62 in^2 and 0.944 in^2, respectively. Although this information is for the West Tower, at the time of model development no information was available regarding the members used in each column of the Central Tower, so the assumption was made that Rodia would have preferred using similar types and sizes of reinforcement. The average area, estimated from the laser scan, of each column around the base of the Central Tower is approximately 14 in^2. Using an average of the two steel members' areas and the estimated cross-section yields a reinforcement ratio of 0.092.

Previous tests completed on the cement mortar reveal that it is fairly consistent with an aggregate-to-cement ratio of 2 1/4-3:1, a compressive strength around 3000-4000 psi, and a unit density of approximately 133 pcf (Ehrenkrantz, 1983). Accounting for the reinforcement, a value

of 145 pcf was used as the material density in the model—a common value for steel reinforced concrete.

ASCE 41-06, *Seismic Rehabilitation of Existing Buildings*, provides recommendations for selecting a lower-bound value for the compressive strength of concrete (f_c') when the material properties are not known. According to ASCE 41-06 Table 6.3, for construction completed between 1920 and 1949, the default lower-bound compressive strength of concrete is between 2000-3000 psi (American Society of Civil Engineers, 2006), which is consistent with the material tests in the Ehrenkrantz report. The initial estimates will conservatively assume a value of 2000 psi. Using the equation for modulus of elasticity in ACI 318-08 §8.5.1 (American Concrete Institute, 2008) yields the following for the concrete modulus of elasticity:

$$E_c = w_c^{1.5} 33 \sqrt{f_c^{'}} = (132.8)^{1.5} 33 \sqrt{2000} = 2.26 \times 10^6 \text{ psi} \qquad (7.1)$$

In the appendix of the Ehrenkrantz report, a set of calculations use a value of 2×10^6 psi for the concrete modulus, but it is not clear what assumptions went into finding this number.

An equally important consideration is the amount of assumed composite action between the steel and concrete, and the amount of moment fixity at each joint. For daily temperature cycles and low-level wind or seismic events, the tower is likely to behave elastically and therefore a high degree of composite action and fixity may be assumed. Although at many locations throughout the tower it is possible that deterioration has reduced the bond between the reinforcing steel and the concrete cover, it was still assumed that the global behavior would be modeled best by using a steel and concrete composite structure. The stiffness of each individual element was therefore based off of a transformed section. The idea behind a transformed section is to convert the steel—which is significantly stiffer than concrete—to an equivalent area of concrete using the transformation ratio, a ratio of the material moduli (Hibbeler, 2008). In order

to find the transformed section, it was assumed that each element was a centrally reinforced member with a constant reinforcement ratio. A value of 29×10^6 psi was assumed for the Young's modulus of steel, giving a transformation ratio of 12.8. The derivation is presented on the following pages.

The variables used in the derivation are:

r = radius of gross cross-section
$r_{s,equiv}$, $r_{ST,equiv}$ = equivalent radius of steel section and transformed steel section
A_g = gross section area
A_s, A_c = area of steel and concrete
ρ = reinforcement ratio = A_s/A_g
E_s, E_c = modulus of elasticity for steel and concrete
n = transformation ratio = E_s/E_c
β = stiffness reduction factor (to account for cracking)
A_{ST}, A_T = transformed area of steel and total transformed area
I_T = transformed second moment of area

1) Compute the gross cross-section area and second moment of area

$$A_g = \pi r^2 \tag{7.2}$$

$$I_g = \frac{\pi r^4}{4} \tag{7.3}$$

2) Compute the area and second moment of area of steel

$$A_s = \rho A_g \tag{7.4}$$

$$r_{s,equiv} = \sqrt{\frac{\rho A_g}{\pi}} = \sqrt{\frac{\rho\pi r^2}{\pi}} = r\sqrt{\rho} \tag{7.5}$$

$$I_S = \frac{\pi r_{s,equiv}^4}{4} = \frac{\pi\left(r\sqrt{\rho}\right)^4}{4} = \rho^2\left(\frac{\pi r^4}{4}\right) = \rho^2 I_g \tag{7.6}$$

3) Compute the area and second moment of area of concrete

$$A_c = A_g - A_s = (1-\rho)A_g \tag{7.7}$$

$$I_c = I_g - I_s = (1-\rho^2)I_g \tag{7.8}$$

4) Compute the steel transformed area and second moment of area

$$A_{ST} = n\rho A_g \tag{7.9}$$

$$r_{ST,equiv} = \sqrt{\frac{n\rho A_g}{\pi}} = \sqrt{\frac{n\rho\pi r^2}{\pi}} = r\sqrt{n\rho} \tag{7.10}$$

$$I_{ST} = \frac{\pi r_{ST,equiv}^4}{4} = \frac{\pi\left(r\sqrt{n\rho}\right)^4}{4} = (n\rho)^2\left(\frac{\pi r^4}{4}\right) = (n\rho)^2 I_g \tag{7.11}$$

5) Compute the final transformed section properties

$$I_T = I_c + I_{ST} = \beta[1 - \rho^2 + (n\rho)^2]I_g \tag{7.12}$$

$$A_T = A_c + A_{ST} = \beta(1 - \rho + n\rho)A_g \tag{7.13}$$

Note that the β term will be initially set as 1.

7.4 Initial Model Results

The model was developed in Abaqus using simple wireframe geometry and two-node linear beam elements (B31 elements in Abaqus). The formulation of B31 elements in Abaqus is based on Timoshenko beam theory, and thus, they can be used for both slender and squat beams (Abaqus, 2012). The mesh was set such that each beam element was approximately 6 inches in length.

With the geometry and section information for the model set, an initial modal analysis was completed in order to check how closely the frequencies matched those retrieved from the acceleration data. The results were surprisingly accurate in the N-S direction with a slightly higher E-W stiffness. In order to reduce the E-W stiffness, the parameter β was set to 0.5 for the beams connecting the East and Center Towers. With this correction, the frequencies matched with reasonable error values between 1% and 15%. The finished model and first mode shape in either direction are shown in Figure 7.7. Table 7.2 summarizes the first three frequencies of the translational modes of vibration, which were obtained from the modal analysis.

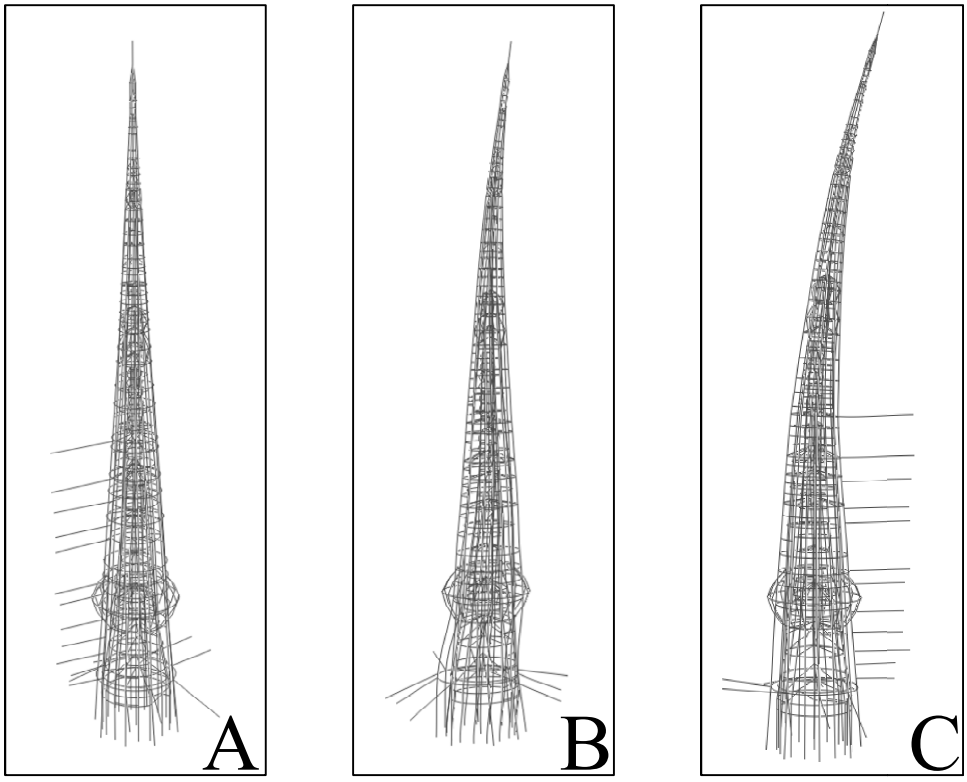

Figure 7.7: A) Finished Abaqus model B) N-S first mode shape C) E-W first mode shape

Table 7.2. Comparison of ABAQUS model and measured frequencies

	North - South			East - West		
	Observed	Model	Error	Observed	Model	Error
f_1	2.25-2.44	2.347	0.30%	2.31-2.65	2.943	14.96%
f_2	3.54-3.97	3.205	-14.08%	3.46-4.37	-	-
f_3	6.31-7.03	5.841	-12.30%	6.75-7.49	6.679	-6.06%

Note that a range of observed frequencies is given, but the percent error is the difference between the frequencies in the model to the average observed frequencies. In the N-S direction—where the structure movements aren't complicated by any coupling—the error in the first mode frequency is less than 1%, indicating an accurate representation of the distribution of mass and stiffness within the model. In the E-W direction, the first mode error is larger, with the model overestimating the frequency by approximately 15%. This could possibly result from modeling the beams connecting the two towers as fixed on the east end, whereas the real condition would involve connecting the beams to another flexible structure. The second mode in the E-W

direction observed in the measurements is absent in the computer model. Again, this could be a problem with overly stiff connecting beams. In order to test the assumptions that went into developing the model, a sensitivity analysis was completed by varying the assumed inputs.

7.5 Sensitivity Analysis

The material density and model geometry can be considered known inputs and therefore will not be varied during the sensitivity analysis. The key inputs that were initially estimated are the stiffness of the concrete and the reinforcement ratio. Recall that the Ehrenkrantz report listed values between 3000-4000 psi for the compressive strength of the concrete. 3000 psi was the upper limit on the range of values recommended in ASCE 41-06. Using this value, the concrete modulus becomes:

$$E_c = w_c^{1.5} 33 \sqrt{f_c^{'}} = (132.8)^{1.5} 33 \sqrt{3000} = 2.77 \times 10^6 \text{ psi}$$

The initial estimate for reinforcement was based on the member sizes that were used in the West Tower. To account for variations in construction, two different values of 5% and 15% were assumed for the reinforcement ratio. The following table shows the resulting frequencies in the model by making these changes.

Table 7.3. Sensitivity analyses with the ABAQUS model

	North - South				East - West			
	Observed	3000 psi	$\rho = 5\%$	$\rho = 15\%$	Observed	3000 psi	$\rho = 5\%$	$\rho = 15\%$
f_1	2.25-2.44	2.365	1.919	2.884	2.31-2.65	2.939	2.439	3.389
f_2	3.54-3.97	3.235	2.640	4.116	-	-	-	-
f_3	6.31-7.03	5.899	4.756	7.553	6.75-7.49	6.333	5.152	7.581

The effect of changing the concrete compressive strength is very limited. Varying the amount of steel has a much more pronounced effect. A 5% reinforcement ratio results in a closer match for the first mode in the east-west direction, but then the stiffness in the north-south

direction is underestimated. A 15% reinforcement ratio results in an overestimate of the frequency in each direction and can be considered somewhat of an upper-bound value. In most cases, the two reinforcement ratios result in frequencies that bound the observed values, meaning the reinforcement ratio likely falls somewhere in between, as the 9% initial assumption does. A rigorous procedure could be developed to vary the input parameters until the errors in each direction were minimized, but it was decided that the initial estimates resulted in frequencies (cf. Table 7.2) that were satisfactorily close to the observed values. The final model was therefore based on a 2000 psi compressive strength of concrete and a 9% reinforcement ratio.

7.6 Thermal Simulations

Modeling the daily tilting behaviors may shed some light on the creation and propagation of cracks. An initial steady-state thermo-elastic simulation was completed by specifying the temperature at one side of the tower and decreasing it linearly across the width of the tower. A thermal expansion coefficient of 1×10^{-5}/°C was assumed for the composite material. Typical values for the thermal expansion coefficient for lightweight concrete range from 6.5×10^{-6}/°C to 1.1×10^{-5}/°C, while reinforcing steel has a coefficient of 1.8×10^{-5}/°C (MacGregor and Wight, 2012). For the initial simulation, the gradient was set with a temperature of 30°C applied to one side of the tower and a temperature of 25°C applied to the opposite side. The reference temperature—i.e., temperature at which the elements are at zero stress—was set to 18°C. The hot side was first set as the north side of the tower, and then the east, with the following results for displacement and rotation. The displacement and rotation values were taken at the nodes along the center column.

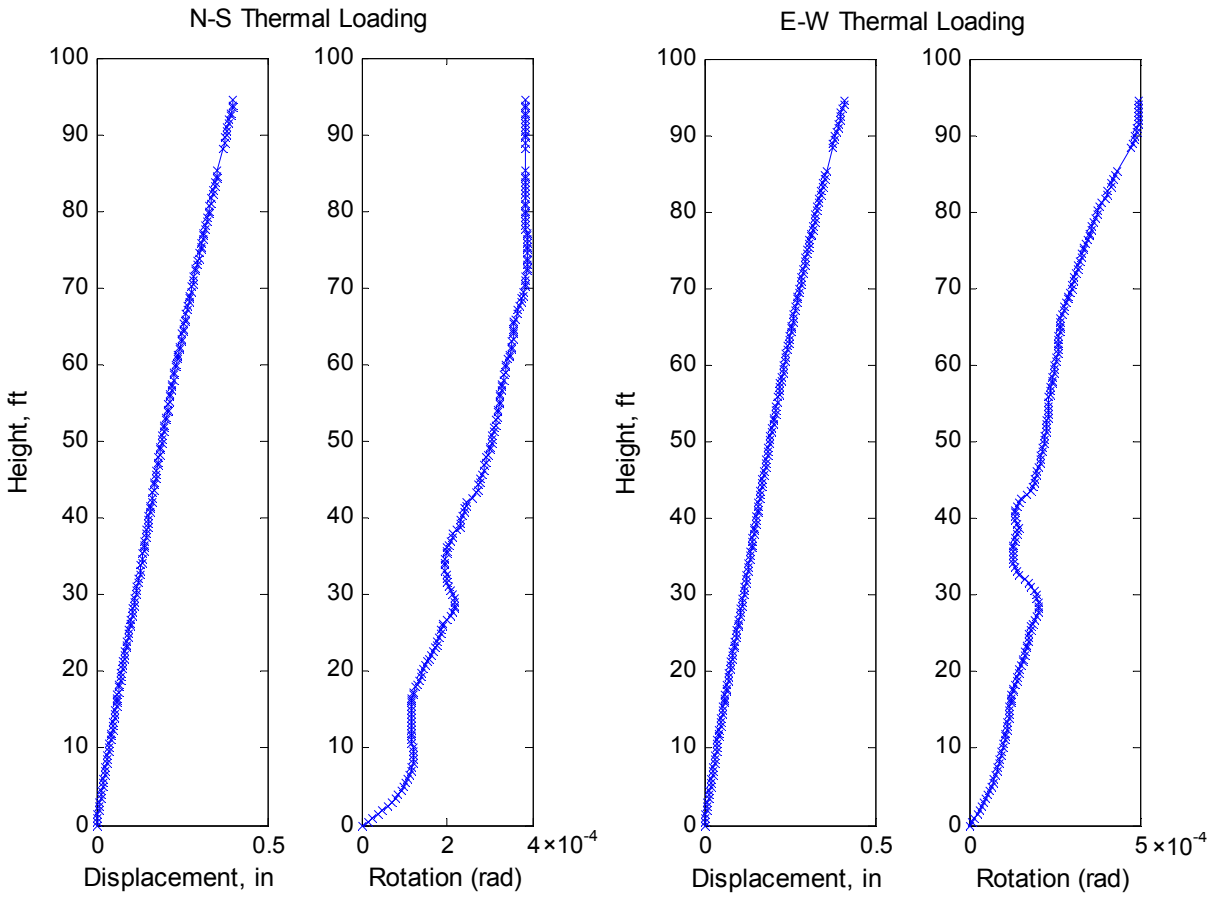

Figure 7.8: Steady state thermal displacement

In both directions, the tip displacement is slightly less than 0.5". The rotation at 23 feet, the location of the tilt meter, is around 2×10^{-4} radians, meaning the peak-to-peak daily rotation would be around 4×10^{-4} radians. The measured tilt values typically ranged between 4×10^{-4} to 9×10^{-4} radians. The rotation falls on the low-end of the observed behavior, but is nonetheless within an order of magnitude. The tip displacement for the N-S simulation was divided by the rotation at 23 feet in order to test the previously derived cantilever approximation (Eq 4.5).

$$\frac{\Delta(x)}{\theta(x)} = \frac{0.0335 \text{ feet}}{1.7 \times 10^{-4}} = 197$$

Recall that the cantilever approximation yielded a ratio of 133. The model yields a higher displacement, which is the expected result given the decreasing flexural stiffness over the height

of the tower. The small rotation values in the model could result from too low of a temperature gradient; the larger the difference between the hot and cold side of the structure, the more it will tilt. The low values may also result from the surface temperature of the tower being hotter than the surrounding air. Over the course of the day, the tower stores thermal energy, causing the material to be much hotter than the surrounding air. With these uncertainties in mind, a simple experiment was devised that consisted of instrumenting the Central Tower with four temperature sensors for a period of a few weeks. This data helps to better define the temperature distribution around the tower throughout the day and night.

7.7 Thermal Monitoring

In order to define the thermal gradient on the tower throughout the day and night, one temperature sensor was attached to the north face of four different columns, one in each quadrant: north, east, south, and west. The sensors were placed on the north side so that they would not be affected by direct sunlight and would more accurately record the surface material temperature. The sensors were attached to the column face via zip tie or Velcro, and then wrapped with an ace bandage, which helped to keep the sensor pressed against the material and insulted from the air. The bandage further helped to thermally insulate the sensor from the effects of direct sunlight. Figure 7.9 shows the locations of the instrumented columns (circled in red) and photographs of one sensor on the east column, before and after wrapping.

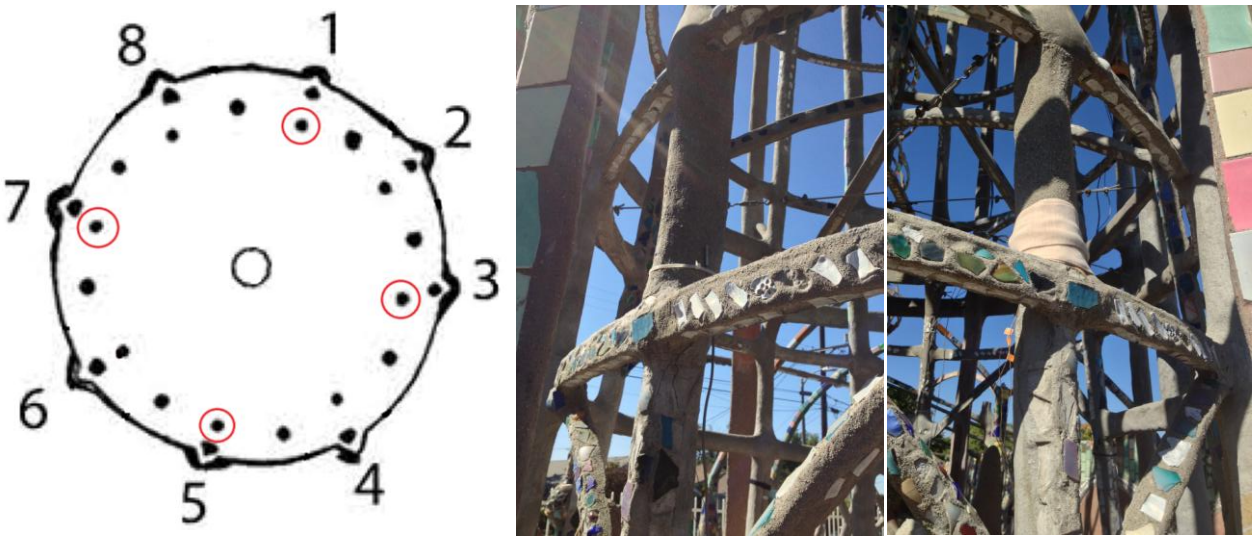

Figure 7.9: Thermal monitoring sensor setup

The sensors used were the TMCx-HD model by Onset Computer Corporation. This model is accurate to within ±0.25°C for temperatures ranging between 0°C to 50°C. (TMCx-HD Documentation, 2013). Each sensor was connected to a HOBO U12 Data Logger, also manufactured by Onset. This data logger can record up to 43,000 events with a 12-bit resolution (U12-008 Documentation, 2011). With four sensors this roughly equates to one sample per minute for a period of one week. The system was set to take one sample every five minutes, meaning it could be left for over a month before the internal memory would run out of space.

This data was collected along with temperature data from a set of four embedded thermocouples that were previously installed on the Central Tower by the LACMA team. The thermocouples were installed on the same east column as selected for the current monitoring. One thermocouple was installed on the surface, with the others installed at depths of 1/2", 15/16", and on the reinforcing steel. Figure 7.10 shows the temperature values from the four sensors around the tower for the first three weeks of monitoring, October 17- November 7. In order to better visualize the daily pattern, Figure 7.11 focuses on only the first two days, October 17 and 18. The thermocouple data is presented in Figure 7.12.

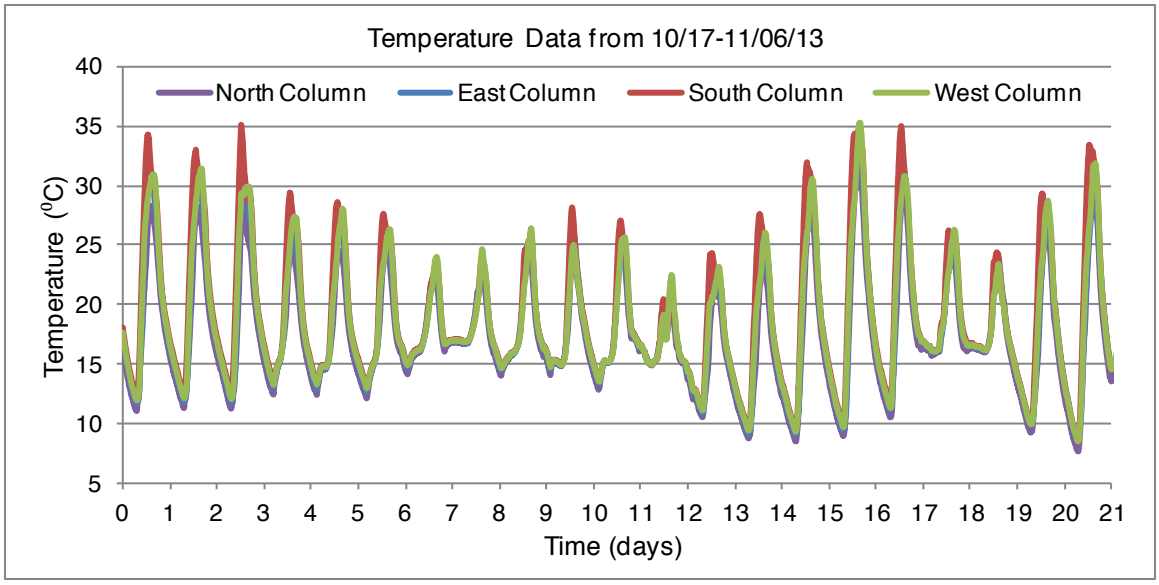

Figure 7.10: Weeks 1-3 thermal monitoring results

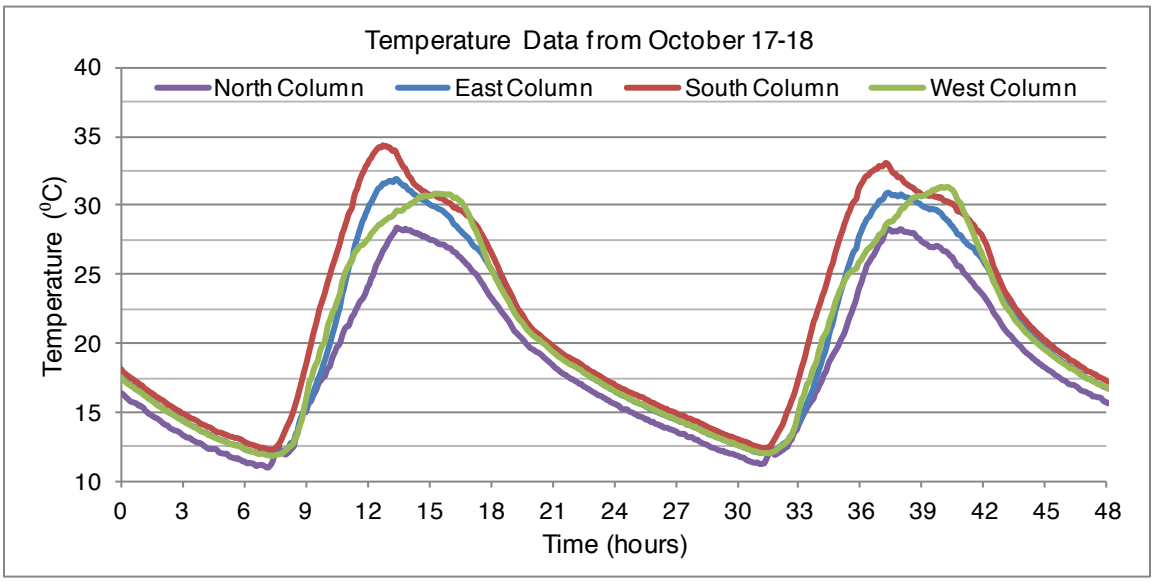

Figure 7.11: Daily temperature distribution around the tower

The temperature follows the expected pattern. The tower continues to cool until sunrise, approximately 7 am. At this point all of the columns are close to the same temperature, and the amount of tilt would be small. Moving forward toward noon, the east and the south column heat up faster than the north or west columns, since they have more exposure to the sun. After 12 pm, the north, east, and south columns all start to cool, whereas the west column continues to slowly heat until around 3-4 pm. Around this time it overtakes the south column as the hottest of the

group. One more thing to note is that the maximum difference between the north and south columns occurs close to noon with a value of roughly 10°C. The difference between the east and west columns is approximately 1-3°C, which seemingly contradicts the previously noticed trend that the east-west tilt was consistently larger than the north-south tilt, despite the fact that the tower is stiffer in the east-west direction. It is possible that the East-to-Center Tower connection plays a role in this behavior, although it is not clear exactly how. On a cool day, a single column may undergo a 10°C temperature change, whereas for the hot days the temperature swings can be as large as 25°C.

One goal of the thermocouple setup was to determine how quickly the heat conducted from the surface to the reinforcing steel. As seen in Figure 7.12 below, there is a very short lag between the surface heating up and the embedded steel reaching its peak temperature. At the high end, the peak embedded steel temperature is around 1-2°C cooler than the peak surface temperature.

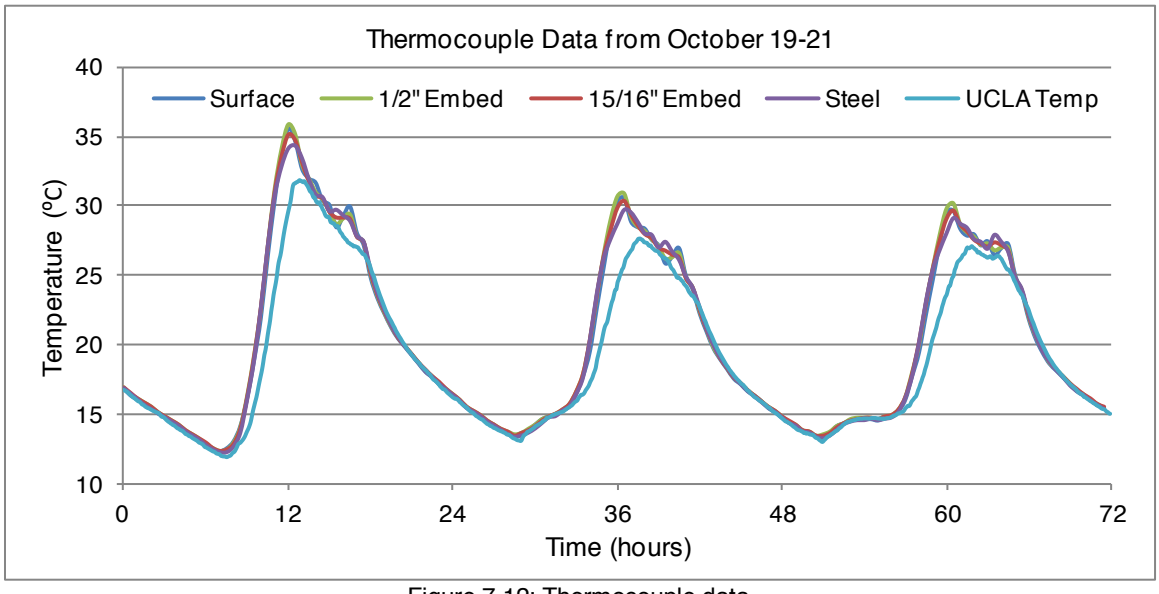

Figure 7.12: Thermocouple data

When compared to the UCLA system, the surface thermocouple is around 3-4°C hotter in the middle of the day. Part of this difference can likely be attributed to the UCLA sensor being placed on the north side of the column, whereas the thermocouples are on the west side and receive more direct sunlight. Overall, the data from the UCLA sensor follow closely with all four of the thermocouples, and therefore can be considered an accurate representation of the surface and internal material temperatures of each column.

7.8 Updated Thermal Simulations

With the temperature data in hand, it was necessary to develop a procedure for defining the thermal loads in the Abaqus model. The first step was to find the hourly-average temperature, breaking down the data into 24 time steps per day. For every time step, the temperature was calculated at each node using a weighted average based on the distance of that node from the (x,y) coordinates of each of the four instrumented columns' base. This procedure is shown below:

Variables:

T_n, T_e, T_s, T_w: Temperature defined at north, east, south, and west columns

(x_n, y_n); (x_e, y_e); (x_s, y_s); (x_w, y_w): coordinates of the columns' base

(x_i, y_i): coordinates of node i

d_{ni}, d_{ei}, d_{si}, d_{wi}: distance from node i to each column

w_n, w_e, w_s, w_w: weighting function applied to each temperature

T_i: temperature at node i

Calculation:

Find distance from node to each column:

$$d_{ni} = \sqrt{(x_n - x_i)^2 + (y_n - y_i)^2}\ ,\ d_{ei} = \sqrt{(x_e - x_i)^2 + (y_e - y_i)^2}\ , \ldots \quad (7.14)$$

Solve for the weighting functions:

$$d_{ni}w_n = d_{ei}w_e = d_{si}w_s = d_{wi}w_w \tag{7.15}$$

where:

$$w_n + w_e + w_s + w_w = 1 \tag{7.16}$$

For example, solving for w_n:

$$w_e = \frac{d_{ni}}{d_{ei}}w_n \ , \ w_s = \frac{d_{ni}}{d_{si}}w_n \ , w_w = \frac{d_{ni}}{d_{wi}}w_n \tag{7.17}$$

$$w_n\left(1 + \frac{d_{ni}}{d_{ei}} + \frac{d_{ni}}{d_{si}} + \frac{d_{ni}}{d_{wi}}\right) = 1 \tag{7.18}$$

$$w_n = \frac{1}{1 + \frac{d_{ni}}{d_{ei}} + \frac{d_{ni}}{d_{si}} + \frac{d_{ni}}{d_{wi}}} \tag{7.19}$$

Finding nodal temperature:

$$T_i = w_nT_n + w_eT_e + w_sT_s + w_wT_w \tag{7.20}$$

It is possible to prescribe a unique temperature to every single node in Abaqus, but this unnecessarily increases the amount of computational effort, with very little increase in accuracy. Therefore, the range of nodal temperatures was separated into different groups based on a half degree separation. For example, group one would include any nodes with temperature values between 11.5-12°C, and group two would include nodes with values between 12-12.5°C, etc. The first week of temperature data were processed using this technique, and the resulting thermal loads were input into Abaqus. Figures 7.13 and 7.14 show the tip displacements of the tower and the rotations of the center column, taken from a node that is at approximately the same height as the tilt sensor.

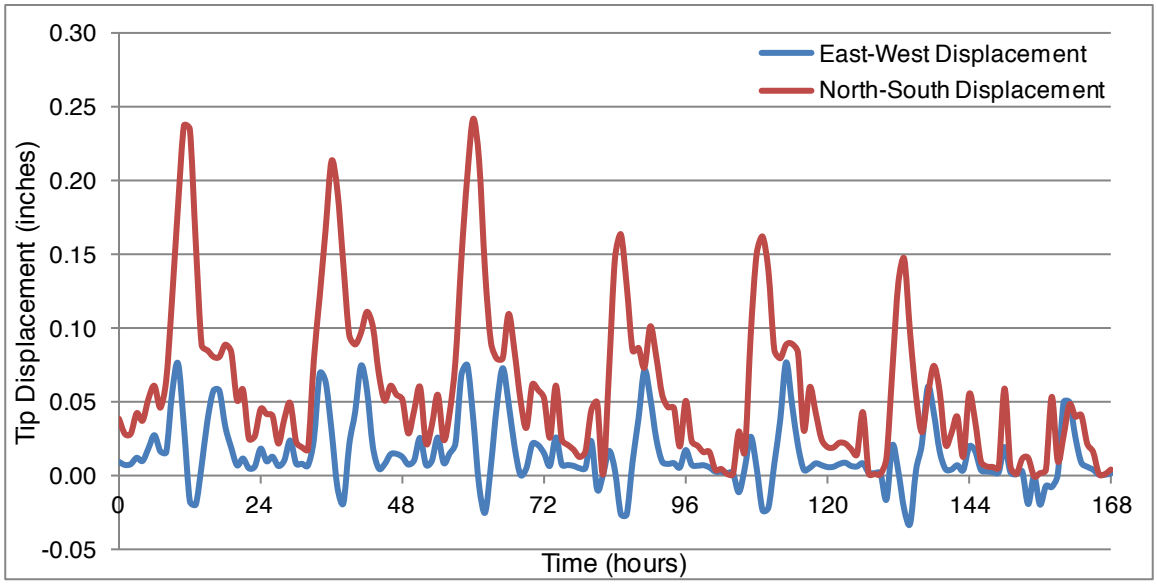

Figure 7.13: Abaqus model tip displacement

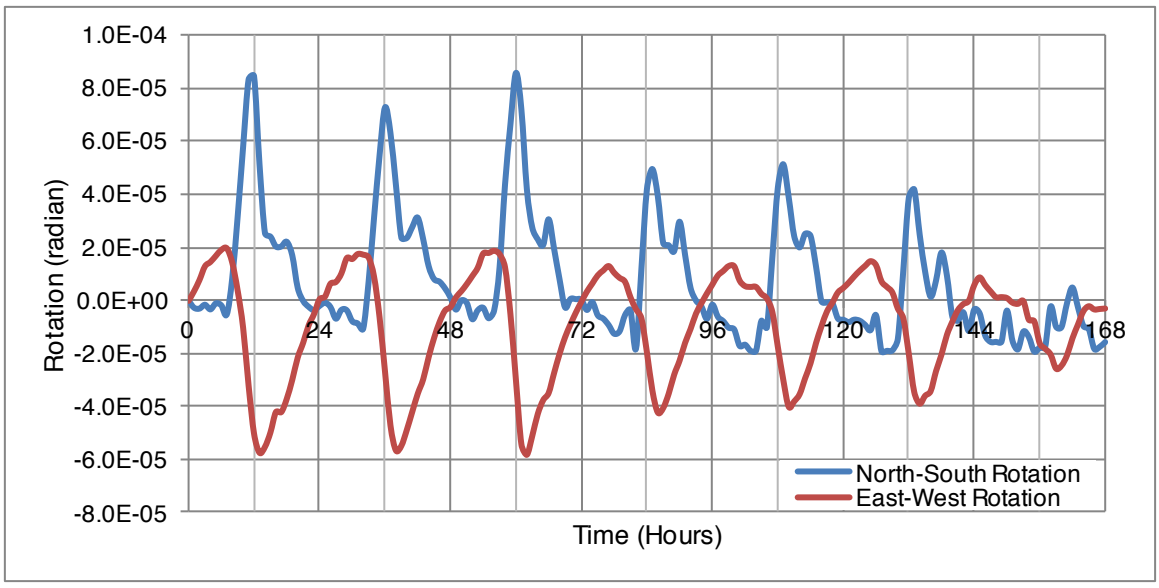

Figure 7.14: Rotation along center core at 23 feet

The tip displacement pattern is more complicated than the tilt pattern, suggesting some type of localized movement of the upper portion of the tower within the model. The rotation approximately follows the previously defined pattern, but again the values are low compared to those that were recorded with the tiltmeter. The peak-to-peak tilt in both the N-S and E-W directions is approximately 8×10^{-5} rad—i.e., one order-of-magnitude smaller than what was measured. The displacements are likewise small, with a peak tip displacement of 0.25” in the

north-south direction. An interesting result to note is that the tilt values are similar in the two directions, but the displacement is much larger in the north-south direction. As was previously noted, during the hotter days, the amount of tilt is quite a bit larger.

One goal of the modeling was to look at the behavior of the two columns that were being monitored for crack movement. Studying the local deformations of these columns can give insight into what type of stresses they are under. The following plots show the displacement of one node from each column that is approximately 7 feet above the base, just below the first horizontal band.

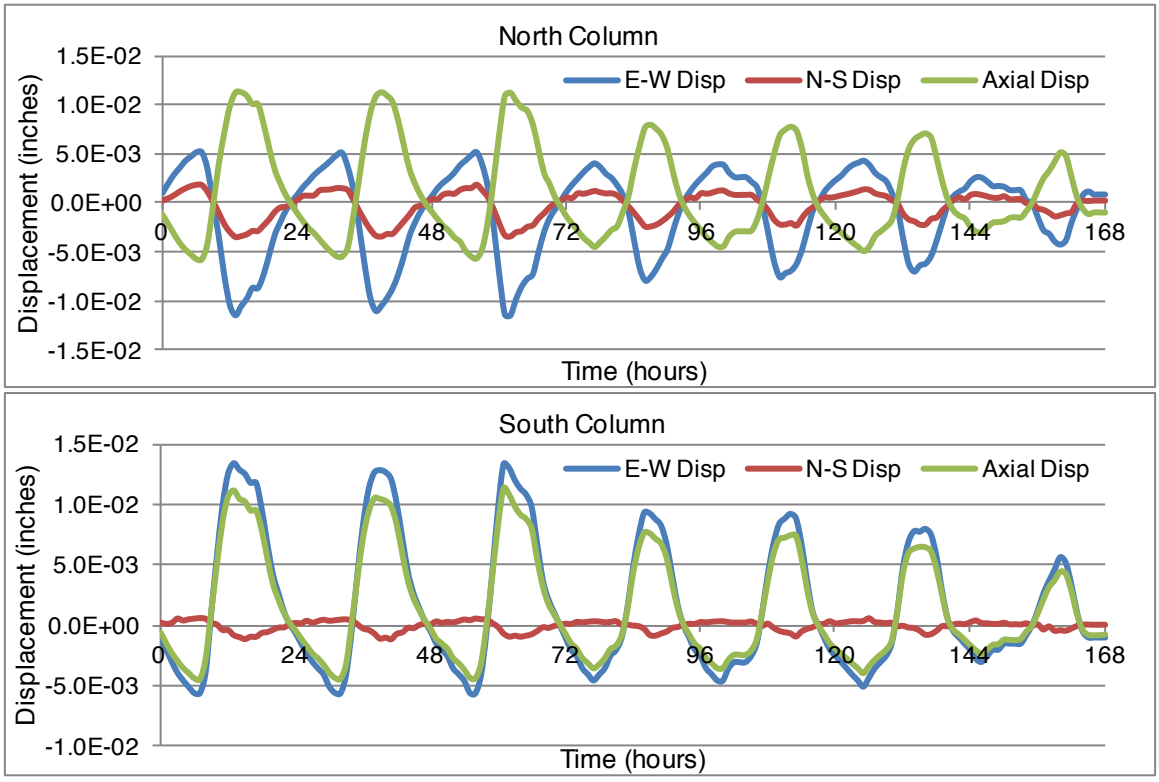

Figure 7.15: North and south column displacements

The axial displacement of both columns is almost exactly equal, which is an expected result since this is largely a function of local expansion. The average strain over the length of the column and the resulting displacement can be calculated as follows:

$$\epsilon = \alpha \Delta t = 1 \times 10^{-5}(22°\text{C}) = 2.2 \times 10^{-4} \tag{7.21}$$

$$\delta = \epsilon L = (2.2 \times 10^{-4})(7 \text{ feet})\left(\frac{12 \text{ inches}}{1 \text{ foot}}\right) = 0.018" \tag{7.22}$$

The difference between the maximum and minimum axial displacements is approximately 0.017", so the results seem consistent. The difference in the two columns' behavior is noticed when looking at the north-south and east-west displacements. For the north column, the E-W and N-S displacements are out-of-phase with the axial displacement. For the south column, the N-S displacement is still out of phase, and much smaller than the axial displacement; but the E-W displacement is in-phase with the axial displacement, and around the same magnitude.

The fact that the two columns' transverse displacements move opposite of each other suggests that the thermal loading may cause some global torsional effects around the base. These transverse displacements will introduce bending stresses in the column. The stresses and strains developed in bending will be along the longitudinal axis, but will lead to small transverse stresses due to Poisson effects. These displacements and strains are fairly small, but it is possible that undergoing these stress levels every day for the past 60 years could cause fatigue cracking to occur. Modeling these fatigue effects can be accomplished by creating a 3D solid model of one of the columns that better represents the actual design and local conditions of the column. This process is, of course, complicated due to the unknown and inhomogeneous design of the elements which make up each tower. The displacement values shown in Figure 7.15 could be used as time-history input for the 3D solid model in order to study the stresses which develop when undergoing these repeated cycles for several years. If cracking is predicted in the model, then it would be reasonable to conclude that these low-level thermal cycles are part of the problem. Additional thermal simulations on the full model can also be completed in order to gain further insight.

8 Summary and Conclusions

The Los Angeles County Museum of Art is currently working toward developing a comprehensive preservation plan for the iconic Watts Towers. As part of their study, LACMA found it necessary to better understand all of the factors that may be contributing to the Tower's deterioration—in particular, the causes of numerous cracks that have formed in the cement mortar. A team from UCLA has provided the expertise to experimentally and analytically study how environmental factors (temperature, wind, and earthquakes) affect one of the tower's global structural behavior and crack movement. Data collected from the Center Tower over the past ten months have provided a wealth of information on the behavior of the tower.

The first mode frequency of the Center Tower is around 2.34 Hz in the north-south direction and 2.56 Hz in the east-west direction. The additional stiffness in the east-west direction is likely due to a coupling effect of the East and Center Towers, which results from a series of twelve beams connecting the two towers at heights between 11 and 45 feet. The observed first mode frequency of the Center Tower varies by approximately 5% during the course of the day in response to changes in temperature. Over the course of several days, the variation is around 8%. The nearly yearlong data set—including temperature data, acceleration measurements, and the extracted frequencies—provides a baseline that can be compared to later measurements in order to study whether the tower's stiffness is decreasing over time. It can also be used to compare with post event measurements, following an earthquake or windstorm, to see if there has been a shift in the structure's frequency due to damage. When comparing data sets, the temperature dependency of the frequency can be minimized using various normalization methods in order to better distinguish whether any observed shifts in behavior are significant.

Over the course of each day, the Center Tower leans away from the sun in response to differential heating. Instrumenting four of the columns around the perimeter of the tower showed that the maximum temperature difference between the north and south columns in the middle of the day was around 10°C. The difference between the east and west columns was smaller—around 3°C. Assuming a uniformly loaded cantilever displacement pattern, the estimated daily peak-to-peak tip displacement using the tilt data is between 1 and 2 inches.

In order to better understand the effects of thermal loading, and to validate the observed tilting behavior, a finite element model of the Central Tower was created in Abaqus. An initial modal analysis of the model in Abaqus resulted in frequencies that matched closely with the observed values from acceleration data. The error in the north-south direction first mode frequency was less than 1%. In the east-west direction, where the motion is complicated by the coupling effect, the error is larger; the first mode in that direction is overestimated by 15%.

The first week of temperature data from the previously mentioned thermal monitoring of the four columns were used as input to define a temperature value at each node in the Abaqus model. The resulting tilt behavior in the model was consistent with what had been observed, but with a few anomalies. The rotation along the center column, at the height of the tilt meter, was approximately 8×10^{-5} radians, an order of magnitude smaller than the measured values. The tip displacements of the center column were likewise smaller than predicted—around 0.25 inches in the north-south direction and 0.1 inches in the east-west direction. The measured tilt values showed consistently larger east-west tilt, whereas the model predicted larger tilt in the north-south direction. Additional thermal simulations using the full data set of temperature values will help to explain the discrepancies between the magnitude of the recorded tilt and the tilt results from the model.

The two instrumented cracks showed consistent daily behavior. The north crack follows an inverse relationship with the temperature; as the temperature increases, the crack closes, with peak daily movement between 0.00014 and 0.00083 inches. During the early stages of monitoring, the north crack showed a gradual opening of approximately 0.003 inches, but it has since remained steadily around a baseline value. This gradual opening was observed, albeit with varying magnitudes, by both the UCLA and LACMA systems and is therefore likely the actual behavior of the crack. The south crack displays a more complicated behavior and greater movement, with peak daily displacements between 0.00017 and 0.0018 inches. Unlike the north crack, the south crack has remained steady around its baseline throughout the entire duration of monitoring. It was hypothesized that direct exposure to sunlight may explain the unique behavior of the south crack. An experiment that involved shading the crack showed a change in the south crack's behavior, but the results were inconclusive. An additional experiment has been proposed that would shade a larger portion of the column and possibly use a small air-conditioning unit to control the local environment. Future data collection may also provide the answer to this question; during a rain storm the amount of direct sunlight would be reduced due to cloud cover, and the rain would help to cool down the structure, minimizing the effects of differential heating.

The two columns that were instrumented to study the cracking were also studied as part of the computer modeling. Looking at the displacements of these columns over the first seven feet, the thermal loading causes axial displacements of 0.02 inches and transverse displacements of approximately 0.015 inches. Although these displacements are small, it is possible that over time this movement can lead to crack formation. If other mechanisms are to blame for the initial crack formation, this daily movement can still be considered as one of the reasons why the cracks continue to persist.

The Watts Towers are located in a seismically active portion of southern California. They are also exposed to regional Santa Ana windstorms, in which northerly winds can reach speeds up to 80 mph. These earthquakes and wind events have been shown to cause damage to the Towers in the past. To date, the level of activity throughout the UCLA monitoring has been small for both earthquakes and winds. Peak accelerations of 0.01*g* were observed during a M4.7 earthquake in March, 2013, with an epicenter approximately 172 km away from the tower. A windstorm in April, 2013, reached peak speeds of around 35 mph, resulting in accelerations of 0.016*g*. These events show that both small earthquakes and moderate wind events produce motions that exceed thermal movement. Data collection will continue, and with some luck, a few larger events will be captured that can help to determine what affect wind and earthquakes have on the tower's long-term behavior.

The main goal of this project is to determine how the environment affects the behavior and deterioration of the Watts Towers. Although not every question has been answered, several key trends have been discovered. At the time that this thesis is submitted, data collection and analysis are still ongoing. The future data collection will hopefully capture larger amplitude earthquake and wind events, as well as rainstorms. The existing computer model can be used to run additional simulations of thermal loading and possibly be updated such that it can be used to predict the response of the tower during an earthquake or wind event. More accurate modeling of local elements where cracking has been observed may provide further insight into the initial causes of cracking. The added data and additional simulations will continue to assist LACMA with their understanding of the behavior of the Watts Towers and will contribute to the long-term preservation of this historical and cultural monument.

References

Abaqus (2012). "Abaqus Theory Manual," Dassault Systemes Simulia Corp., Providence, RI.

ACI Committee 318 (2008). *Building Code Requirements for Structural Concrete (ACI 318-08) and Commentary (318R-08),* American Concrete Institute, Farmington Hills, MI.

ANCO (1988). *Final Report: Simon Rodia Towers Environmental Measurements – Phase I*, prepared for the City of Los Angeles, ANCO Engineers Inc., Culver City, CA 90232, May 1988.

ANCO (1989). *Final Report: Simon Rodia Towers Environmental Measurements – Phase II*, prepared for the City of Los Angeles, ANCO Engineers Inc., Culver City, CA 90232, April 1989.

American Society of Civil Engineers (2006). *ASCE/SEI Standard 41-06, Seismic Rehabilitation of Existing Buildings*, Reston, VA.

American Society of Civil Engineers (2010). *ASCE/SEI Standard 7-10, Minimum Design Loads of Buildings and Other Structures*, Reston, VA.

Applied Geomechanics (2001). "Model 716-2 Wall Mount Tiltmeter Spec Sheet". Accessed August 2013. http://nees.org/data/get/facility/sensorModels/164/Documentation/tiltmeter%20spec%20sheet.pdf

Asghari A (2009) *Characterization of Environmental Variability in Identified Dynamic Properties of a Soil-Foundation-Structure System*, PhD Dissertation, University of Southern California

Bendat JS, Piersol AG (1993) *Engineering Applications of Correlation and Spectral Analysis*, (2nd ed.). John Wiley & Sons, Inc. New York, NY.

California Geological Survey (2013). "About CSMIP," California Department of Conservation. Accessed September 2013, http://www.consrv.ca.gov/CGS/smip

CGS-California Geological Survey (2007). *Integrated Tri-Axial Accelerograph, State of California System Requirements*, CGS/DGS SYSREQ 2007-TR

Chopra AK (2007). *Dynamics of Structures*, (3rd ed.), Pearson Prentice Hall, Upper Saddle River, NJ.

Clinton JF, Bradford SC, Heaton TH, Favela J (2006). The Observed Wandering of the Natural Frequencies in a Structure. *Bulletin of the Seismological Society of America*, 96(1): 237-257.

Dassault Systemes (2013). "Abaqus Overview", Abaqus Unified FEA. Accessed September, 2013. http://www.3ds.com/products-services/simulia/portfolio/abaqus/overview/

Doebling SW, Farrar CR, Prime, MB (1998). A Summary Review of Vibration-based Damage Identification Method. *Shock and Vibration Digest*, Vol. 30, No. 2, 91-105.

The Ehrenkrantz Group/Building Conservation Technology (1983). *Preservation Plan: Simon Rodia's Towers in Watts*. Los Angeles, CA

Encyclopedia of Science (2002). "Phototropism", accessed September 2013 http://www.encyclopedia.com/topic/Phototropism.aspx

Farrar CR, Doebling SW, Cornwell PJ, Straser EG (1997). Variability of modal parameters measured on the Alamosa Canyon Bridge. *Proc*. *IMAC 15* (Orlando, FL, February 1997) pp 257–63

Farrar CR, Duffey TA, Doebling SW, Nix DA (1999). A Statistical Pattern Recognition Paradigm for Vibration-Based Structural Health Monitoring. *2nd International Workshop on Structural Health Monitoring*, Stanford, CA, September 8-10.

Firstmark Controls (2013). "World's Smallest Cable Position Transducer, Specs," accessed August 2013, http://www.firstmarkcontrols.com/s021f.htm

Friswell MI, Penny JET, Wilson DAL, (1994). Using Vibration Data And Statistical Measures to Locate Damage In Structures. *Modal Analysis: The International Journal of Analytical and Experimental Modal Analysis*, Vol. 9, No. 4, pp. 239–254.

GBG USA (2013). "Laser Scanning, Mobile Laser Scanning," accessed August 2013, http://www.gbg-us.com/#!__laser-scanning-tech

Gill Instruments (2013). "WindObserver 65: Ultrasonic Anemometer, Data Sheet," accessed August 2013, www.gillinstruments.com/data/datasheets/WindObserver65.pdf

Goldstone B, Goldstone AP (1997). *The Los Angeles Watts Towers*, Los Angeles: Getty Conservation Institute and J. Paul Getty Museum. Los Angeles, CA

Goldstone NJ (1963). Structural Test of Hand-Built Tower, *Experimental Mechanics*, 3(1), 8-13.

Hale W (Director), (1957).*The Towers*. Produced by Rembrandt Films

Harris FJ (1978). On the Use of Windows for Harmonic Analysis with Discrete Fourier Transformation, *Proceedings of the IEEE*. Vol 68, No. 1, p. 51.

Hemez, FM, Farhat C (1995). Structural Damage Detection via a Finite Element Model Updating Methodology, *Modal Analysis -- The International Journal of Analytical and Experimental Modal Analysis*, Vol. 10, No. 3, pp. 152-166

Hibbeler RC (2008). *Mechanics of Materials*, (7th ed.), Pearson Prentice Hall, Upper Saddle River, NJ.

Kinemetrics (2013). "EpiSensor ES-T: Force Balance Accelerometer, Data Sheet," accessed August 2013, http://www.kinemetrics.com /uploads/PDFs/EPISENSOREST.pdf

Los Angeles County Museum of Art. (2011-2013). "Watts Towers Quarterly Progress Reports," accessed September 2013, www.lacma.org/art/exhibition/watts-towers

Los Angeles County Museum of Art (2012). *Preliminary Vibration Monitoring Study - Santa Ana Wind Event,* internal memo

MacGregor JG, Wight JK (2012). *Reinforced Concrete: Mechanics and Design* (6th ed.), Pearson, Upper Saddle River, NJ.

Matlab (2013). "MATLAB Documentation Center," accessed August 2013, www.mathworks.com/help/

Matlab (2009). "MATLAB File Exchange," *Vectorized Solar and Azimuth Elevation*. Written by: Darin Koblick. Feb 2009. Accessed September 2013, www.mathworks.com/matlabcentral/ fileexchange/23051-vectorized-solar-azimuth-and-elevation-estimation

National Oceanic and Atmospheric Administration (2013). "LIDAR-Light Detection and Ranging," accessed September 2013, http://www.oceanservice.noaa.gov/facts/lidar.html

Newmark NM, Hall WJ (1982). *Earthquake Spectra and Design*, Earthquake Engineering Research Institute, Berkeley, CA

Onset Computer Corporation (2011). "HOBO U12 4-External Channel Outdoor/Industrial Data Logger (Part #U12-008) Spec Sheet," accessed October 2013, http://www.onsetcomp.com/ products/data-loggers/u12-008

Onset Computer Corporation (2011). "TMCx-HD Water/Soil Temperature Sensor, Spec Sheet," accessed October 2013, http://www.onsetcomp.com/products/sensors/tmc20-hd

Quanterra (2013). "Quanterra Q330 Spec Sheet," accessed August 2013, www.Q330.com

Rytter A (1993). *Vibration based inspection of civil engineering structures*, PhD Dissertation, Department of Building Technology and Structural Engineering, Aalborg University, Denmark

Skolnik D (2008). *Building Instrumentation*, PhD Dissertation, Department of Civil and Environmental Engineering, University of California Los Angeles.

Sohn H, Farrar CR, Hunter NF, Worden, K (2001) "Structural Health Monitoring Using Statistical Pattern Recognition Techniques," *Journal of Dynamic Systems, Measurement, and Control*, 123(4), 706-711.

University of California San Diego (2013). "May Gray/June Gloom," accessed November 2013, http://meteora.ucsd.edu/cap/gloom.html